Multiplexed and Micropatterned 3 Dimensional (3D) GelMA Platform as an *in vitro* model for Oligodendrogenesis

by

Ecem Metin

A Dissertation Submitted to the
Graduate School of Health Sciences
in Partial Fulfillment of the Requirements for
the Degree of

Master of Science

in

Cellular and Molecular Medicine

January 15, 2024

Multiplexed and Micropatterned 3 Dimensional (3D) GelMA Platform as an *in vitro* Model for Oligodendrogenesis

Koç University

Graduate School of Health Sciences

This is to certify that I have examined this copy of a master's thesis by

Ecem Metin

and have found that it is complete and satisfactory in all respects,
and that any and all revisions required by the final
examining committee have been made.

Committee Members:

Assist. Prof. Emel Sokullu (Advisor)

Prof. Arzum Erdem Gürsan

Prof. Ayşe Altıntaş

Date: 15.01.2024

For my father

ABSTRACT

Multiplexed and Micropatterned 3 Dimensional (3D) GelMA Platform as an *in vitro* Model for Oligodendrogenesis

Ecem Metin

Master of Science in Cellular and Molecular Medicine

January 15, 2024

The occurrence of disturbances in myelination can lead to the development of a range of disorders. A reliable and biologically mimicking *in vitro* model of oligodendrogenesis is of necessity to aid in elucidating the pathogenesis of demyelinating diseases. Oligodendrogenesis and myelination are highly dependent on the function of extracellular matrix (ECM) components. The recent advancements in biomaterials illustrated that hydrogels have tremendous potential to mimic the ECM of central nervous system (CNS). It remains elusive whether the characteristics of hydrogels can manage to regulate the differentiation and maturation of oligodendrocyte (OL) lineage cells and provide a suitable model without the need for primary cells or *in vivo* models. Here, this study examines the impact of a multiplexed and micropatterned 3 Dimensional (3D) Gelatin Methacrylate (GelMA) platform on the viability, and spheroid formation of Human Oligodendroglioma (HOG) cells under different UV exposure conditions, while also exploring the maturation status. Both proliferation and spheroid formation were enhanced with prolonged UV exposure durations, illustrating the importance of ECM dynamics on cellular behaviour. The cell viability on day 5 was the greatest at 50 seconds of exposure condition. The formation of spheroids was discernibly observed on day 5 at exposure conditions of 40 and 50 seconds, with the latter showing a notable effect. Maintenance in GelMA induced the mRNA expression of transcription factors OLIG2, SOX2 and SOX10; OPC markers PDGFRα and NG2; and OL markers CNPase, MBP, and MOG. The expression of GFAP was not detected in the case of 3D whereas it was found to be traceably expressed in 2D cultured cells, suggesting a possible rescue from astrocyte lineage in 3D. Immunofluorescence microscopy confirmed the expression of MBP and MOG at the protein level. These results imply the regulatory effect of the GelMA environment on the expression profile of HOG cells, altering their fate towards OL lineage. To ascertain whether alterations in the expression of OL genes are exclusive to 3D maintenance, a separate treatment of UV and GelMA was applied to HOG cells cultured in a 2D environment. Neither UV treatment nor GelMA addition made significant changes on the expression profile of HOG cells. In conclusion, this platform appears to be a noteworthy culture model for oligodendrogenesis, warranting further investigation. Coculture of SH-SY5Y cells with HOG cells was conducted to see if any interaction would occur. Although SH-SY5Y cells were not differentiated into mature neurons, their interaction with HOG cells was evident, leading to accumulation near HOG spheroids with the latter crosslinking exhibiting a notable effect. Further investigation with the usage of mature neurons and oligodendrocyte lineage cells within the hydrogel may aid in enlightening whether the platform also serve as a model for myelination.

Key words: Oligodendrocytes, oligodendrogenesis, 3D-hydrogel Model, GelMA, myelination

ÖZETÇE

Oligodendrojenez Modellemesi için 3 Boyutlu (3B) Çoklu ve Mikropaternli GelMA Platformu

Ecem Metin

Hücresel ve Moleüler Tıp, Yüksek Lisans

Ocak 15, 2024

Miyelinizasyon mekanizmasındaki aksaklıklar, çeşitli bozuklukların gelişimine yol açabilir. Demiyelinizan hastalıkların patogenezini aydınlatmaya yardımcı olmak için güvenilir ve biyolojik olarak mimike edebilen bir in vitro miyelinizasyon ve oligodendrojenez modeline ihtiyaç vardır. Oligodendrojenez ve miyelinizasyon, ekstrasellüler matris (ESM) bileşenlerinin fonksiyonuna son derece bağlıdır. Biyomalzemelerdeki son ilerlemeler, hidrojellerin merkezi sinir sistemi (MSS) ESM'sini taklit etme potansiyeline sahip olduğunu gösterdi. Hidrojellerin özelliklerinin, oligodendroglial (OL) hücrelerinin diferansiyasyonunu ve olgunlaşmasını düzenleyip düzenleyemediği ve primer hücrelere veya in vivo modellere ihtiyaç duyulmadan uygun bir model sağlayıp sağlayamadığı henüz belirsizdir. Bu çalışma, farklı UV maruziyet koşulları altında İnsan Oligodendroglioma (HOG) hücrelerinin yaşayabilirlik ve sferoid oluşumu üzerinde multipleks ve mikropaternli bir 3 Boyutlu Jelatin Metakrilat (GelMA) platformunun etkisini incelemekte ve aynı zamanda olgunlaşma durumunu araştırmaktadır. Hem çoğalma hem de sferoid oluşumu, uzun UV maruziyet süreleri ile arttı, bu da ESM dinamiklerinin hücresel davranış üzerindeki önemini göstermektedir. Gün 5'te hücre yaşayabilirliği, 50 saniyelik maruz kalma koşulunda en yüksek oldu. Sferoid oluşumu, 40 ve 50 saniye maruziyet koşullarında gün 5'te belirgin bir şekilde gözlemlendi, sonuncusunun anlamlı bir etki gösterdiği görüldü. GelMA'da kültür, OLIG2, SOX2 ve SOX10 transkripsiyon faktörlerinin; OPC markerlerinin, PDGFRα ve NG2; ve OL markerlerinin CNPase, MBP ve MOG'u indükledi. GFAP ekspresyonu, 3B durumunda tespit edilmedi, ancak 2B kültüre edilmiş hücrelerde izlenebilir şekilde ifade edildi, bu da 3B ortamında astrosit kökeninden kurtuluşun mümkün olabileceğini düşündürmektedir. İmmünoflorasan mikroskopisi, MBP ve MOG'un protein düzeyinde ifadesini doğruladı. Bu sonuçlar, GelMA çevresinin HOG hücrelerinin ekspresyon profili üzerinde düzenleyici bir etkisi olduğunu, kaderlerini OL kökenine doğru değiştirdiğini ima etmektedir. OL genlerinin ekspresyonundaki değişikliklerin 3B bakımına özgü olup olmadığını belirlemek için, UV ve GelMA'nın ayrı bir muamelesi, 2B ortamında kültüre edilmiş HOG hücrelerine uygulandı. Ne UV tedavisi ne de GelMA eklemesi, HOG hücrelerinin ekspresyon profili üzerinde anlamlı değişikliklere neden olmadı. Sonuç olarak, bu platform, oligodendrojenez için dikkate değer bir kültür modeli gibi görünmektedir ve daha fazla araştırmayı hak etmektedir. SH-SY5Y hücrelerinin HOG hücreleri ile ko-kültürü, herhangi bir etkileşimin olup olmadığını görmek amacıyla gerçekleştirildi. SH-SY5Y hücreleri olgun nöronlara diferansiye edilmediği halde, HOG hücreleri ile etkileşimleri belirgindi ve özellikle HOG sferoidlerine yakın birikim gösterdi. Hidrojel içinde olgun nöronlar ve oligodendrosit hücreleri kullanarak yapılacak

daha fazla araştırma, platformun miyelinizasyon modeli olarak da hizmet edip edemeyeceğini aydınlatmada yardımcı olabilir.

Anahtar Kelimeler: Oligodentrosit, oligodendrojenez, 3B- Hidrojel Model, GelMA, miyelinizasyon

AKNOWLEDGEMENTS

I would like to express my gratitude to Dr. Emel Sokullu for her invaluable contributions to the completion of my thesis. Furthermore, I want to extend my gratitude to Nilufar Ismayilzada, Melike Kocahasan and Mohammad Haroon Qureshi who played remarkable roles as my research collaborators throughout my master's research.

Last but not least, I would also like to convey my sincere appreciation to Deren Demirel, for her encouragement and emotional support during this journey. Her unwavering belief in me served as a root of my motivation. To Nurperi Berfin İskenderoğlu, the 'mirror' of myself, your presence has made the struggles more bearable.

Most importantly, thank you for your interest and hope in this research dad. My mother, you have been a friend and the best mother throughout not only my academic life but also "my whole life".

Thank you all.

Ecem

TABLE OF CONTENTS

LIST OF TABLES

LIST OF FIGURES

ABBREVIATIONS

CNS	Central Nervous System
MS	Multiple Sclerosis
ADEM	Acute-disseminated encephalomyelitis
AHL	Acute Hemorrhagic Leucoencephalitis
PML	Progressive Multifocal Leukoencephalopathy
CPM	Central Pontine Myelinolysis
OPCs	Oligodendrocyte precursor cells
PNS	Peripheral Nervous System
MS	Multiple Sclerosis
AD	Alzheimer’s Disease
ALS	Amyotrophic Lateral Sclerosis
PD	Parkinson’s Disease
PLP	Proteolipid Protein
MBP	Myelin Basic Protein
CNPase	2',3'-cyclic nucleotide 3'-phosphodiesterase
MAG	Myelin-associated glycoprotein
MOG	Myelin Oligodendrocyte Glycoprotein
myOLs	mature myelinating oligodendrocytes
OPCs	Oligodendrocyte progenitor cells
OL	oligodendrocyte
PDGFRα	platelet-derived growth factor receptor α
SVZ	Subventricular zone
ECM	Extracellular matrix
CSPGs	Chondroitin sulfate proteoglycans
HSPGs	Heparan Sulfate Proteoglycans
GAG	glycosaminoglycans
HA	hyaluronic acid
GelMA	Gelatin Methacrylate
3D	three-dimensional

2D	two-dimensional
SCI	Spinal cord injuries
TBI	Traumatic brain injuries
VEGF	Vascular endothelial growth factor
hMSCs	Human mesenchymal stem cells
BDNF	Brain-derived neurotrophic factor
HOG	Human oligodendroglioma
MAA	Methacrylic Anhydride
TMSPMA	3-(trimethoxysilyl)propyl methacrylate
PI	photoinitiator
Irgacure 2959	2-Hyroxy-4′-(2-hyroxyethoxy) -2-methylpropiophenone
SEM	Scanning Electron Microscopy
UV	Ultraviolet
DMSO	Dimethyl sulfoxide
PFA	Paraformaldehyde
PEG	Polyethyleneglycol

Chapter 1:
INTRODUCTION

Myelination is a crucial biological process that enables the maintenance of optimal neuronal function by rapid saltatory nerve conduction. The occurrence of disturbances in myelination can lead to the development of a range of devastating neurological disorders, namely demyelinating and dysmyelinating diseases. Demyelinating diseases are characterized by the gradual damage and loss of the myelin sheath that surrounds axons. Demyelination within the central nervous system (CNS) could be due to several mechanistic abnormalities originating from inflammatory responses, nerve entrapments, ischemia, and alterations in metabolism (Love, 2006). Etiologically, the role of environmental factors including stress, viral agents, vitamin D levels, diet, heavy metal poisoning, and tobacco smoking has been broadly underlined (Donati, 2020; Haase et al., 2018; Maiuolo et al., 2019; Rosso and Chitnis; Spanier et al., 2015; Stohlman and Hinton, 2001). Some examples of demyelinating diseases include multiple sclerosis (MS), acute-disseminated encephalomyelitis (ADEM), acute hemorrhagic leucoencephalitis (AHL), progressive multifocal leukoencephalopathy (PML), central pontine myelinolysis (CPM), and more (Love, 2006). Among them, multiple sclerosis (MS) is the most common form, with an estimated incidence rate of 2.1 per 100,000 persons/year and a prevalence of 35.9 per 100,000 people (Walton et al., 2020).

Dysmyelinating conditions are another branch of myelin disorders and are characterized by defective metabolism affecting myelin assembly, causing hypomyelination or dysmyelination. They are genetic disorders of myelin, in distinction to demyelinating conditions that are mostly acquired (See recent review: Duncan and Radcliff, 2016). Defects of myelin have been shown to be present also in neurodegenerative diseases like Alzheimer’s Disease (AD), Amyotrophic lateral sclerosis (ALS) (Kang et al., 2013), and Parkinson’s disease (PD). Ota et al. (2019) demonstrated that the myelin density is significantly decreased in the left hippocampus, left insula, right precuneus, and bilateral anterior cingulate of AD patients relative to healthy subjects. In another study, abeta pathology, a major hallmark of Alzheimer's disease (AD), was associated with grey matter demyelination (Mitew et al., 2010). Myelin damage was suggested to be the potential origin of neuropathological abnormality in AD. In human

brain samples obtained from patients with AD braak stage (I/II), the temporal cortex displayed a reduction in the activity of ceramide synthase 2 (CERS2), one of the fundamental players in myelin biosynthesis (Couttas et al., 2016). Cognitive and behavioral impairment in PD has been associated with the aberrant function of the cingulate cortex (Palermo et al., 2018; Zhou et al., 2021). Analysis of RNAseq data of the cingulate cortex from PD patients has revealed significant downregulation of genes corresponding with myelination and oligodendrogenesis, suggesting a possible contribution of the myelination network to cognitive symptoms of PD (Xie et al., 2022).

1.1 The Composition of Myelin Sheath

Myelin sheath is evolutionarily conserved among vertebrates, underscoring it as a fundamental component of the nervous system (Zalc et al., 2008). The myelin sheath functions as an insulator of axons by providing trophic support to sustain rapid impulse propagation alongside the neurons. In fact, as the action potential “jumps" from one Ranvier node to another, it is estimated that signal transmission is accelerated up to 100-fold by virtue of myelin sheath (Fields and Dutta, 2019). The composition of myelin sheath includes specific proteins and lipids. The in-situ water content of myelin is about 40%, in which the remaining dry mass is featured by a high proportion of lipid (70 to 85%), whereas 15 to 30% of protein. Such composition is remarkably unique to myelin considering the fact that the majority of biological membranes possess a greater ratio of proteins to lipids (Morell and Quarles, 1999). The most abundant protein constituent of CNS myelin is proteolipid protein (PLP), a 30-kDa lipophilic, a four-span transmembrane protein, accounting for about 40% by weight of the protein content of myelin (Kister and Kister, 2023; Greer and Lees, 2002; Morell and Quarles, 1999; Nave et al., 1987; Stoffel et al., 1984). Both in vitro and in vivo experiments demonstrated that myelin membrane adhesion and compaction in the CNS are coordinated by the adhesive properties of the proteolipid protein (Bakhti et al., 2014; Palaniyar et al., 1998; Ruskamo et al., 2022). The proteolipid protein gene (PLP1) encoding for PLP was reported to be holding a high degree of conservation (Kitagawa et al., 1993). PLP1 has 7 exons with a length of 17 kb and is localized at the proximal long arm of the X chromosome, Xq21-q22 (Mattei et al., 1986). Missense, deletion/insertion, and splice-site mutations and duplications of the gene are associated with Pelizaeus-Merzbacher disease (PMD), also called leukodystrophy

hypomyelinating 1 (HDL1), and spastic paraplegia 2 (SPG2) disorder (Hodes et al.1993; Raskind et al., 1991). The severity of PMD has been correlated with PLP1 mutation, explaining the critical role of PLP in myelination and myelin stability (Hobson and Garbern, 2012; Wolf et al., 2005). Similarly, Warshawsky et al. (2005) associated the phenotypic characteristics of primary progressive multiple sclerosis with Leu30Arg (c.89TG) mutation in proteolipid protein.

The second most abundant protein in CNS myelin is 18.5-kDa isoform myelin basic protein (MBP), with a proportion of 30% by weight of the myelin proteins (Kister and Kister, 2023). MBP is recognized as the primary responsible protein involved in myelination (Baumann and Pham-Dinh, 2001). The compaction of myelin and both paranodal and juxtaparanodal integrity were shown to be highly reliant on MBP biosynthesis (Meschkat et al., 2022). Moreover, the stability of axon-glia interactions during myelination is tailored by MBP (Bakhti et al., 2014).

Another constitutional protein of myelin sheath is 2',3'-cyclic nucleotide 3'-phosphodiesterase (CNPase), a membrane-anchored myelin enzyme that gives rise to 3–4% of protein weight, making it the third most abundant protein in CNS myelin (Raasakka and Kursula, 2014). Compared to MBP, little is established about its function in myelination. Nevertheless, the absence of CNPase in transgenic mice models was shown to be causing subsequent axonal swelling and neural death (Lappe-Siefke et al., 2003). Studies on cultured oligodendrocytes (OLs) obtained from CNPase-deficient mice have demonstrated the critical role of CNPase in OL support through interactions with the cytoskeleton during myelination (Lee et al., 2005).

Although their quantification is minor, it is worth mentioning the glycoprotein constituents of myelin sheath: MAG (myelin-associated glycoprotein) and MOG (myelin oligodendrocyte glycoprotein). MAG is not present in the compact myelin but in oligodendroglial membranes near axons. Most likely owing to its location, it functions in the adhesion of mature oligodendrocytes to axons, and signaling dynamics between (Yin et al., 1998; Pronker et al., 2016). The association of MAG dysfunction with myelination diseases has been well recognized, indicating its non-negligible role in myelination even its low quantity (Wajgt and Gorny, 1983; Lossos et al., 2015; Aboul-Enein et al., 2003). Similarly, MOG is present on the membranes of oligodendrocytes as well as on the surface of myelin sheath. This has also been suggested to be attributable to the potential function of MOG as a cell surface receptor or cell adhesion molecule (Martini and

Schachner, 1986). Since the earlier studies, it was reported that MOG is a differentiation marker for oligodendrogenesis (Linington et al., 1988).

1.2 Key regulators of Oligodendrogenesis

The assembly of the myelin sheath, myelination, is reliant upon the proper positioning, maturation, and proliferation of oligodendrocytes in the CNS. The collection of multilamellar extensions of mature myelinating oligodendrocytes (myOLs), oligodendrogenesis, gives rise to the formation of myelin sheath. The process of oligodendrogenesis involves the creation of oligodendrocytes in the developing and adult brain. It is essential for replacing damaged oligodendrocytes, maintaining myelin plasticity, and regenerating myelin following demyelination in CNS (Fletcher et al., 2021). The development of myOLs is directed by a precise program involving the maturation of oligodendrocyte progenitor cells (OPCs). OPCs, also called NG2-glia (due to the expression of NG2 proteoglycan on the cell surface) or polydendrocytes (named after their multi-characteristics) (Dimou and Gallo, 2015), are distinguished from other CNS cell residents by means of their electrophysiological characteristics and expression of specific genes. In contrary to the linear electrophysiological profile of astrocytes and mature oligodendrocytes, OPCs have unique and highly complex electrophysiology, such as the presence of voltage-gated ion channel currents, ligand-gated ionotropic neurotransmitter receptors and their capability to receive synaptic input from neurons (Clarke et al., 2012; Lin and Bergles, 2004). The stage-specific gene expression profile of OPCs primarily involves platelet-derived growth factor receptor α (PDGFRα), NG2 chondroitin sulphate proteoglycan, SOX10, O4 antigen, and the basic helix-loop-helix transcription factors OLIG1 and OLIG2, which all are known to be essential for regulating key stages of early oligodendrocyte development (for recent reviews, see Wegner, 2008; Bergles and Richardson, 2016). Expression of OLIG1 and OLIG2 is upregulated in response to induced expression of the class II transcription factors Nkx6.1 and Nkx6.2 in differentiating neuroepithelial stem cells by Sonic hedgehog (Shh) (Nery et al. 2001; Wegner 2008). The importance of the expression of OLIG2 and PDGFRα in oligodendrogenesis and their regulation by Shh is thoroughly proposed by Nery et al. (2001). Nkx2.1 mutant mice had produced telencephalic Shh negativity which in return resulted in the absence of early expression of both OLIG2 and PDGFRα within the ventral

telencephalon, suggesting the requirement of adequate regulation of the Shh pathway for OLIG2 and PDGDRα expression, thereby, oligodendrocyte specification in vivo. In another study, Zhou and Anderson (2002) emphasized the absolute need for OLIG1 and OLIG2 expression for oligodendrocyte commitment. Oligodendrocyte specification lineage is disrupted in Olig1/2 double-mutant mice, where pMN progenitors of the spinal cord generated V2 interneurons and astrocytes instead of oligodendrocytes. The underlying mechanism of the activity of OLIG2 in lineage specification is extensively studied in literature. For instance, OLIG2 dimerizes with E2A proteins to induce SOX family transcription factors, namely SOX9 and SOX10 expression (Akay et al., 2021). Especially, the collaboration between OLIG2 and SOX10 is essential for early oligodendrocyte development. In the CNS, the expression of SOX10 is elevated during the development of glial precursor cells into OPCs, and it is shown to be persistently expressed over oligodendrocyte differentiation and maturation (Stolt et al., 2002). In the early postnatal subventricular zone (SVZ), neural stem cells are driven to mature into oligodendrocytes by the interplay between Sox8, Sox9 and, Sox10 (Pozniak et al., 2010). Among SOX families, the role of SOX2 can be considered as the most elusive and controversial. In vitro levels of Sox2 in OPCs have been reported to be absent (Kondo and Raff, 2004; Lyssiotis et al., 2007), whereas constant low expression is found to be present in vivo (Dai, et al., 2015). Shen et al. (2008) proposed that SOX2 aids in the maintenance of OPC proliferation yet has an inhibitory role in oligodendrocyte (OL) differentiation and regeneration. Zhao et al. (2015) provided an insight within this context, elucidating the function of SOX2. It appeared that although its role in developmental myelination in the postnatal spinal cord is “dispensible”, the recruitment of OPCs to the demyelinated areas of the spinal cord for myelin repair is sustained by SOX2.

1.3 ECM of CNS and Oligodendrogenesis

Oligodendrogenesis and myelination are highly dependent on the function of extracellular matrix (ECM) components of CNS. In the context of CNS, the ECM refers to the space between neurons and glial cells that accounts for about 20% of the total volume of the brain (Benarroch, 2015). The ECM of CNS is predominantly composed of Chondroitin sulfate proteoglycans (CSPGs) (aggrecan, versican, neurocan, brevican, phosphacan), Heparan Sulfate Proteoglycans (HSPGs), and glycosaminoglycans (GAG), (mainly hyaluronan, hyaluronic acid (HA), families), and basement membrane proteins (collagen, laminin, nidogens (enactins), and fibronectin) (Zimmermann and Dours-Zimmermann, 2008; Rowlands et al., 2015). The interaction between OL lineage cells with basement membrane proteins was reported to be essential for maturation and differentiation of these cells, and their myelination capacities. Laminin was shown as a crucial promoter of the survival of OPCs and a determinant factor on the morphology of OL lineage cells. Transgenic mice where the Lama2, the gene that encodes the laminin α2-subunit, was deleted displayed decreased survival of OPCs and defects in myelination (Relucio et al., 2012). The interaction between integrin β1 and laminin α chains positively regulates the migration of OPCs along blood vessels (Suzuki et al., 2019). To the contrary with laminin, fibronectin and hyaluronic acid are negative regulators of oligodendrogenesis and myelination. Accumulation of fibronectin in demyelinated plaques is present, attributed to the inhibition of the oligodendrocyte differentiation and remyelination (Stoffels et al., 2013). Qin et al. (2017) proposed the exogenous treatment of GD1a as a potential therapeutic for demyelination since it modulates the inhibiting affect of fibronectin aggregation. Likewise, HA accumulation in white matter is detected and shown to be a responsible component for OPC arrestment, preventing its differentiation and subsequent remyelination in dysmyelinating disorders (Bugiani et al., 2013). A recent study demonstrated the inhibitory role of hyaluronic acid and its allied receptor CD44 in the morphological differentiation of OL progenitor cells, suggesting it is a main contributory mechanism involved in the accumulation of degraded HA products within the focal demyelinating lesions in MS patients (Sato et al., 2022).

The exact function of collagen in oligodendrogenesis has been poorly defined until recently. Discoidin domain receptor 1, a ligand of collagen IV, is highly expressed in OL lineage cells (Vilella et al., 2019). Research investigating its function divulged that Ddr1

facilitates OL differentiation and myelination (Franco-Pons et al., 2006; Mei et al., 2023). Morphogenesis of OLs was demonstrated when OLs were incubated with collagen IV, credited for the DDR1 and MBP upregulation (Silva et al., 2023). This cumulating evidence suggests collagen IV as a positive modulator for OL fate determinant as opposed to fibronectin and HA. The role of CNS-ECM components on oligodendrogenesis and myelination is summarized in Table 1. It is worth mentioning that the employed hydrogel in this study, Gelatin Methacrylate (GelMA), is modified from gelatin, which is the hydrolyzed product of collagen. Like collagen, gelatin possess the Arg-Gly-Asp (RGD motif) sequence and the matrix metalloprotease (MMP) targeting sequence, favoring cell adhesion, and ECM remodeling (Yin et al., 2022). These make GelMA an attractive biomaterial for CNS tissue engineering (Loessner et al., 2016).

Table 1. The role of CNS ECM components in Oligodendrogenesis and Myelination

COMPONENT	IMPORTANCE
Laminin	⊕ OPC proliferation (Relucio et al., 2012) ⊕ OPC migration (Suzuki et al., 2019) ⊕ myelination (Relucio et al., 2012).
Collagen	⊕ OPC differentiation (Mei et al., 2023) ⊕ myelination (Franco-Pons et al., 2006) (Silva et al., 2023)
Fibronectin	⊕ OPC proliferation (Stoffels et al., 2015) ⊖ OPC differentiation (Stoffels et al., 2013) ⊖ myelination (Sisková et al., 2006)
Hyaluronic acid (HA)	⊖ OPC differentiation (Sato et al., 2022) ⊖ myelination (Bugiani et al., 2013)

1.4 Biomaterials in Mimicking ECM of CNS

The recent advancements in biomaterials have illustrated that they have a tremendous potency to mimic extracellular matrix, which can consequently provide proper cell migration, localization, survival, and differentiation (Cramer and Badylak, 2019; Levenberg et al., 2003). In such a context, hydrogels are considered to be ideal candidates owing to their unique characteristics. Hydrogels are defined as a three-dimensional (3D) network of polymer chains giving rise to multi-component systems with an ability of water retain between macromolecules (Ahmed, 2015). 3D hydrogel models were demonstrated as physiologically recapitulating platforms to study glioma biology as they preserve the cell–cell, and cell–matrix interactions that resemble in vivo (Shah et al., 2021). Also, studies concerning spinal cord injuries (SCI) and traumatic brain injuries (TBI) shown potential applications of hydrogels in CNS tissue engineering and regeneration, given their biomimetic properties. For instance, TBI rats that are treated with Vascular endothelial growth factor (VEGF) incorporated collagen/heparin scaffold displayed improvement in motor functions, neuro-inflammation, and brain edema (Zhang et al., 2021). For similar purposes, Park et al. (2010) modified HA with laminin-derived IKVAV peptide and Brain-derived neurotrophic factor (BDNF). The formed HA-scaffold containing differentiated Human mesenchymal stem cells (hMSCs) was then implanted into rat SCI models. Consequently, the hydrogel was degraded, releasing BDNF, and led to locomotor recovery.

Gelatin methacrylate (GelMA) hydrogels, a modified gelatin with methacyrolyl groups, have particularly attracted the widespread interest of researchers because of their excellent water retention properties, biocompatibility, biodegradability, and moldability. The effect of the GelMA environment on cell behavior, especially its tunable characteristics like stiffness, is broadly established in glioblastoma studies (Fan et al., 2015; Nguyen et al., 2016). However, until recently a few studies indicate the effect of 3D hydrogel scaffolds on OPC survival, oligodendrogenesis, and myelination. Russell and Lampe (2017) demonstrated that the survival and morphology of MADM cells, cells that express many markers of OPCs, are contingent upon hydrogel swelling and stiffness. They have encapsulated OPCs with Polyethyleneglycol (PEG) based hydrogel in which the size and concentration of PEG vary. The proliferation of OPC and commitment to oligodendrocyte lineage were higher in more compliant and more crosslinked conditions,

respectively. In hyaluronic acid-based hydrogels, lower hydrogel stiffness, with the decreased concentration of norbornene-modified hyaluronic acid, facilitated higher levels of cell viability and larger cell spheroid formation by MADM cells (Unal et al., 2020). Only one study explored the transcriptional effect of a hydrogel scaffold on OPCs. By compared to aforesaid studies, Nakano et al. (2023) employed primary OPCs and assessed their proliferation and differentiation characteristics in 2D versus 3D collagen matrix. It was reported that OPCs display a less mature genotype in 3D conditions than the ones conventionally cultured. Within the 3D context, their proliferation rate increased in scaffolds with lower collagen densities compared to in those with higher densities. Overall, these findings indicate the importance of biomaterial properties in oligodendrocyte fate.

Attempts on elucidating the cellular and molecular mechanisms of oligodendrogenesis have been reliant on primary human oligodendrocytes. However, the reproducibility of this method is limited due to the scarcity of available and viable human brain tissue. Therefore, OPC-resembling cell lines like MADM, HOG (Human oligodendroglioma), and MO3.13 have been used in 2D culture exposed to various differentiation conditions, however; the results were inconsistent (Buntinx et al., 2003; De Kleijn et al., 2019). Hence, a need for a novel in vitro platform, resembling in vivo conditions, remains to monitor oligodendrogenesis and to further aid in enlightening underlying cellular and molecular mechanisms. Based on the previously mentioned studies, it is right to say there is a huge gap in the literature concerning the interaction between 3D scaffolds and oligodendroglial cells. Moreover, as aforesaid, findings on 2D culturing of cell lines, particularly HOG cells, were controversial. Given that, it remains elusive whether the characteristics of hydrogels can manage to regulate the differentiation and maturation of such cell lines and provide a recapitulating model without the need for primary cells. Here, this study utilizes HOG cells, a clonal cell line derived from a surgically removed human oligodendroglioma (Post and Dawson, 1992). HOG cells have been used in studies concerning oligodendrocyte differentiation in vitro (Schoenfeld et al., 2010; Gomez-Pinedo et al., 2022), auto-inflammation (Buntinx et al., 2004), viral infection (Bello-Morales et al., 2012), and neurotoxicity (Martínez-Pinilla et al., 2021). This current study investigates the effect of a multiplexed and micropatterned 3D GelMA platform with different conditions, on the viability and spheroid formation. Maturation status of Human Oligodendroglioma (HOG) cells within the hydrogel is also explored.

Chapter 2:
METHODOLOGY

2.1 Cell Maintenance

Human Oligodendroglioma Cell Line (HOG), a tumor-derived cell line, is kindly provided by Prof Dr Alaattin Şen (Department of Molecular Biology and Genetics, Abdullah Gul University, Kayseri, Turkey). The cells were expanded in DMEM-High Glucose (Sigma Aldrich, Cat. No. D6429), supplemented with 10% heat-inactivated FBS (Biowest) and 1% Penicillin-Streptomycin solution (Biowest, Cat. No. L0022) and incubated at 37 ^{0}C with 5% CO_2. Cell passage was mediated every three days at 1:6 splitting with 0.25% Trypsin-EDTA (Multicell, Cat. No. 325-043-EL). SHSY-5Y cells, a cloned subline of a neuroblastoma cell line from a metastatic bone tumor, were expanded in DMEM-F12 (Multicell, Cat. No. 319-085-CL) which is supplemented with 10% FBS and 1% Penicillin-Streptomycin solution and incubated at 37 ^{0}C with 5% CO_2. Cell passage was mediated every three days at 1:10 splitting with 0.25% Trypsin-EDTA.

2.2 GelMA synthesis

GelMA (ZetaMatrix) was synthesized by using the One Pot Method. (Shirahama et al., 2016). Briefly, gelatin (10%) (w/v) in carbonate-bicarbonate buffer (0.25 M, pH = 9) was dissolved and reacted on a magnetic stirrer for 2 hours at 45 ^{0}C. Methacrylic Anhydride (MAA) (MAA/gelatin = 0.1/1 (ml/g)) was slowly added to the mixture and stirred at 500 rpm (Figure 2.2a). The reaction proceeded on a magnetic stirrer, at 50 ^{0}C for 3 hours. Then, the pH of the solution was adjusted to 7.4 in order to terminate the reaction. After being filtered, the solution was dialyzed with 10–14 kDa cut-off membranes for a week in distilled water to remove salts, unreacted MAA compounds, and other byproducts. The clarified GelMA solution was stored at –20 ^{0}C for 2 hours then at -80 ^{0}C for at least 12 hours. The polymer solution was then lyophilized for a week and the ultima freeze-dried product, GelMA foam, was stored at –20 ^{0}C until further usage (Figure 2.2b).

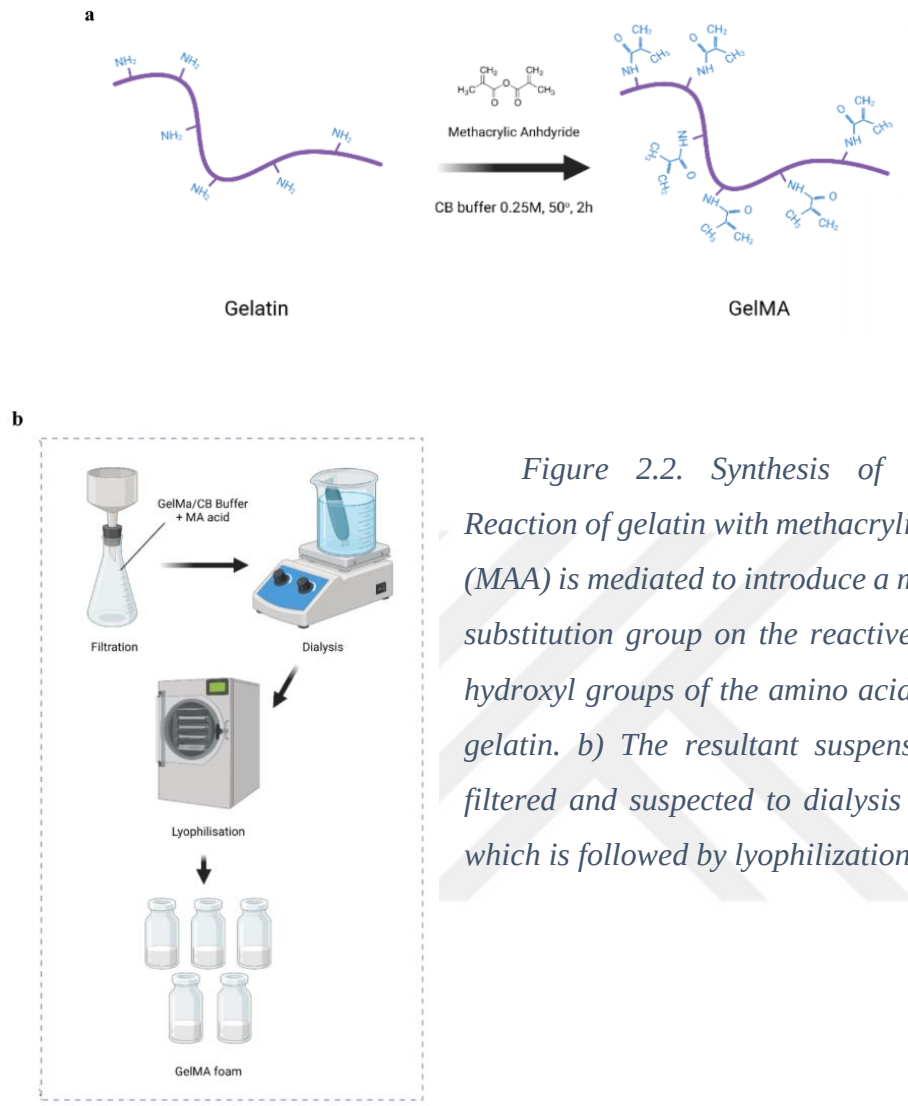

Figure 2.2. Synthesis of GelMA. a) Reaction of gelatin with methacrylic anhydride (MAA) is mediated to introduce a methacryloyl substitution group on the reactive amine and hydroxyl groups of the amino acid residues of gelatin. b) The resultant suspension is then filtered and suspected to dialysis for a week, which is followed by lyophilization.

2.3 Surface Treatment of Coverslips

The adhesion of GelMA to coverslips (18x18 mm) (ISOLAB) was enhanced by acrylation, which was achieved using 3-(trimethoxysilyl)propyl methacrylate (TMSPMA) (Sigma-Aldrich, Cat. No. 440159). The protocol provided by Ersoy and Sokullu (2019) was employed. Coverslips were dipped into a 10% (w/v) sodium hydroxide (Merck, Germany) solution for 1.5 hours, followed by triple washing with distilled water and drying in a vacuum oven. Then, coverslips were treated with TMSPMA overnight at 80 ^{0}C. The treated coverslips were rinsed with absolute ethanol 3 times and let dry in a laminar flow hood. The coverslips were kept at room temperature prior to the experiments and used within a week after acrylation.

2.4 Preparation of pre-polymer solution

Pre-polymer solution was prepared by using a photoinitiator (PI) 2-Hyroxy-4′-(2-hyroxyethoxy)-2-methylpropiophenone (Irgacure 2959) to later initiate photopolymerization under UV, during encapsulation. PI was dissolved in DPBS (1%) (w/v) at 80 ^{0}C. 5% (w/v) GelMA was added to the solution and incubated at 37 ^{0}C. The mixture was then filtered (0.2 μm) and either immediately used or was covered with aluminium foil and refrigerated at 4 ^{0}C until further use (Sawyer et al., 2016).

2.5 Scanning Electron Microscopy (SEM)

The morphological properties of photo-crosslinked GelMA were observed by Zeiss Ultra Plus Field Emission Scanning Electron Microscope (FE-SEM). Pre-polymer solution was exposed to UV for different durations: 30, 40, and 50 seconds. Two constructs were generated from each group of exposure time within a given biological replicate. Non-crosslinked solution was washed away with DPBS, and the remaining 3D hydrogel construct(s) was submerged in a 1 ml of DBPS to allow swelling. After 2 hours, DPBS was removed by aspiration, and the constructs were kept at -20 ^{0}C for 2 hours. Following that, they were transferred to -80 ^{0}C and kept overnight. The frozen GelMA constructs were lyophilized for 24 h before imaging. Samples were sputtered with 25 nm of gold. Imaging was performed at the electron high tension (EHT) of 3.00 kV with a working distance of (WD) 6 mm. Quantification of pore sizes was executed by the image processing software ImageJ and exported as a list. From the list, 250 values were randomly selected, and subsequent analyses were done.

2.6 Green fluorescent protein (GFP) and Red fluorescent protein (RFP) tagging

Lentiviral mediated transduction was used for fluorescent labeling of the cells. HEK-293T cells were used to package pLenti CMV GFP Puro plasmid (Addgene # 17448) and Plenti-CMV-MCS-RFP-SV-puro (Addgene #109377) plasmids using cotransfected psPAX2 and pMD2.G plasmids. Supernatants containing viruses were used for transduction on HOG (GFP) and SH-SY5Y (RFP) cells.

2.7 Encapsulation of HOG cells

HOG cells were trypsinized when they reached 80% confluency. Following the inactivation of trypsin, centrifugation at 800 g took place for 5 minutes. Desired amount of cell suspension was added into a new falcon, which was exposed to recentrifugation at the same conditions. The supernatant was aspirated, and the pellet was mixed within the pre-polymer solution, containing GelMA foam + PI (Figure 2.7a), with a desired density of cells (either 1, 2, or 4 million/ml). The passage numbers of HOG cells were between 8 and 15. The prepolymer solution, containing cells, were cured for 30, 40, and 50 seconds using The OmniCure S2000 UV 12 Light Curing System (365 nm) (Excelitas Technologies Corp., Waltham, MA, USA). Doughnut-shaped photomasks were put on the covered cell/pre-polymer to obtain 3D micropatterned hydrogel constructs (Figure 2.7b). The amount of cell/prepolymer solution was 20 µl for each construct. Photomasks were drawn with a graphical design software (CorelDRAW, Corel corp., Canada) and printed out by A Print, Izmir, Turkey. UV curation was from 50 mm in which the power density was set to 5, 25 W/cm2. The thickness of each construct has been arranged to 0.3 mm. After the UV exposure, the non-crosslinked solution was meticulously washed away employing cell-grade DPBS. Following DBPS washing, a gentle wash with culture medium was done. The requisite amount of medium, 2 ml on each well of 6-well plate, was gently added onto encapsulated cells and was put into an incubator until further assays. The culture medium was changed every other day.

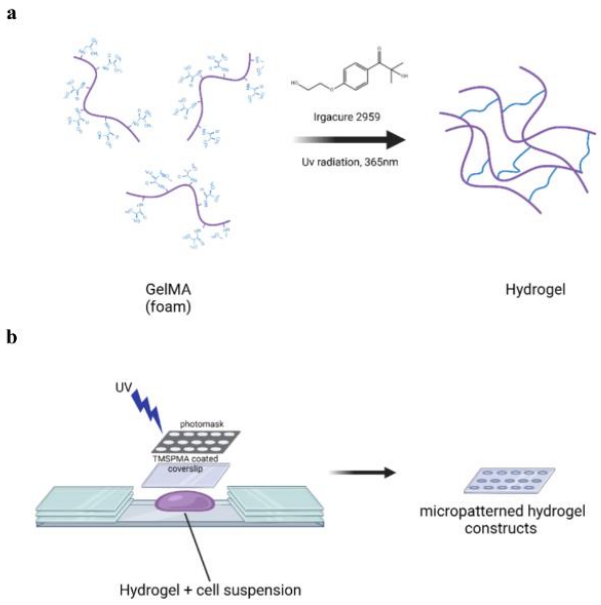

Figure 2.7. Schematic representation of Encapsulation a) Prepolymer solution is obtained via the mixture of GelMA foam in Irgacure 2959/PBS, in which the desired amount of Human Oligodendroglioma (HOG)/or SH-SY5Y cells (See section 2.7) are dissolved. b) Photo crosslinking, by virtue of photomasks, took place to form multiplexed-micropatterned hydrogel constructs under UV irradiation (365 nm) (5.25 W/cm^2).

2.8 Encapsulation of SH-SY5Y cells

SH-SY5Y cells were trypsinized when they reached 80% confluency. Following the inactivation of trypsin, centrifugation at 400 g took place for 5 minutes. Desired amount of cell suspension was added into a new falcon, which was exposed to recentrifugation at the same conditions. The supernatant was aspirated, and the pellet was mixed within the pre-polymer solution with a desired density of cells (either 0.5, 1, or 1.5 million/ml). Photopolymerization was achieved by the aforementioned method (Section 2.7) with an alteration of exposure durations, which were 40, 50, and 60 seconds. After the UV exposure, the non-crosslinked solution was washed away employing cell-grade DPBS. The requisite amount of medium, 2 ml on each well of 6-well plate, was gently added onto encapsulated cells and was put into an incubator until further assays. The culture medium was changed every other day.

2.9 Cell Viability Assays

The viability of HOG and SH-SY5Y cells within three-dimensional gel constructs was assessed using MTT ((3-(4,5-Dimethylthiazol-2-yl)-2,5-Diphenyltetrazolium Bromide) (Invitrogen, Cat. No. M6494). MTT stock solution (5 mg/ml) in cell grade DPBS was prepared and added into the serum-free medium at a concentration of 10 % (as the final volume of each well of a 6 well-plate to be 1.5 ml) and incubated at 37 ^{0}C for 4 h. The solution was removed and 1 ml of cell grade DMSO (Dimethyl sulfoxide) (PanReac AppliChem, Cat. No. A3672) was added. The sample was incubated for 25 mins prior to the measurement of the optical density values of the wells at 570 nm, using BioTek, Synergy H1 Hybrid Reader.

2.10 RNA Isolation and Reverse Transcription

For the quantification of respective gene expressions, HOG cells were maintained in 2D and 3D conditions. HOG cells were encapsulated with a cell density of 4 mn/ml, and the aforementioned UV exposure settings were followed, with 50 seconds of exposure. The selection of 4 mn/ml aims to optimize conditions for the upcoming RNA isolation experiments, focusing on maximizing RNA yield. A total of three 3D-hydrogel constructs were prepared. RNA of 2D-maintained HOG cells was isolated when they reached 80% of confluency, which was attained two days after the initial seeding of 10^5 cells into per well of a 6-well culture plate. RNA isolation was performed with NucleoSpin RNA, Mini kit for RNA purification (Macherey-Nagel) following the instructions of the manufacturer. The cells were trypsinized and centrifuged at 800 g for 5 min. The subsequent cell pellet was dissolved with DPBS and re-centrifuged at the same conditions. The supernatant was removed with aspiration. In a separate tube, a mixture containing 350 µl Buffer RA1 (Lysis Buffer) and 3.5 µl ß-mercaptoethanol (ß-ME) (100X, 55 mM in DBPS) (Gibco) was prepared and added onto the cell pellet with gentle pipetting. The working area and pipettes were cleaned with RNaseZap (Ambion) before proceeding.

RNA isolation protocol for 3D conditions was optimized with slight changes to the standard method. The medium covering the 3D constructs was aspirated, followed by DBPS washing to remove medium-based contaminants. Such a step is particularly crucial in 3D since hydrogels retain the culture medium, which may lead to reduced RNA yield and purity if not thoroughly removed. Initial mechanical disruption of hydrogels was forced using a 10 µl pipette tip. Then, a lysis solution containing 500 µl RA1 and 5 µl ß-ME was added to all constructs, and vigorous pipetting was performed. The lysate was transferred into a cryovial and snap-freezed with liquid nitrogen. The frozen sample(s) was thawed at room temperature. Following thawing, the sample was passed through a 21-gauge needle with a 2-ml syringe for about 25 times. The lysates obtained from both 2D, and 3D conditions were placed into spin columns provided by the manufacturer and processed using the given protocol. The concentration and the quality of obtained RNA were determined by Thermo Scientific™ NanoDrop™ 2000/2000c Spectrophotometer. 150 ng of RNA was reverse transcribed using M-MLV reverse transcriptase (200 U/µl) (Invitrogen, Cat. No. 28025013). The resultant cDNA was not diluted, the final volume was 25 µl.

2.11 Real Time-quantitative PCR

The expressions of MBP, CNPase, MOG, PDGFRα, NG2, OLIG2, SOX2, SOX10, and GFAP were analysed using real time quantitative polymerase chain reaction (RT- qPCR). RT-qPCR were performed in a final volume of 20 µl consisting of 1 × SYBR Green qPCR master mix (QIAGEN, Germany) and 0.5 µM forward and reverse primers, and 2 ul of cDNA using Roche LightCycler 480. The “no cDNA” sample was processed in parallel with the others and tested for each pair of primers to prevent any possible contamination. For those, 2 ul of nuclease free water was put instead of cDNA. All primers were designed using Primer Blast software, confirmed in UCSC Genome Browser and synthesized by Macrogen, Europe. Beta Actin (ACTB) was used as a housekeeping gene to normalize the expression levels. The $2^{(-\Delta\Delta\ CT)}$ method was used for the calculation of gene expressions.

All primers were designed in the sequences provided on the next page.

Table 2. Sequence of primers used for qPCR

Gene	Primer Sequence 5'-3'
MBP	ACCCAAGATGAAAACCCCGTA
	TCCGTAGCCAAATCCTGGTCT
CNPase	CGTGCTGCATTGCACAACCAAG
	CTTGCGTGTCACAAAGAGGGCA
MOG	TTTTGATCCCCACTTTCTGAGG
	CGTAGCTCTTCAAGGAATTGCC
PDGFRα	AGGTGGTTGACCTTCAATGG
	TTTGATTTCTTCCAGCATTGTG
SOX2	AGCTACAGCATGATGCAGGA
	GGTCATGGAGTTGTACTGCA
SOX10	GGCTGCTGAACGAAAGTGA
	TCTTGTAGTGGGCCTGGATG
OLIG2	GCTGCGTCTCAAGATCAACA
	GCTGCGTCTCAAGATCAACA
NG2	GTCCTGCCTGTCAATGACCAAC
	CGATGGTGTAGACCAGATCCTC
GFAP	CTGGAGAGGAAGATTGAGTCGC
	ACGTCAAGCTCCACATGGACCT
ACTB	GACAGGATGCAGAAGGAGATCAC
	GCTGATCCACATCTGCTGGAA

2.12 Immunofluorescence Staining

To see if MBP and MOG are present at the protein level, immunofluorescence staining was performed. HOG cells that are maintained in 2D or 3D conditions were treated. For 3D, the constructs were washed with DPBS 3 times for 1 minute each washing. For 2D, the cover glasses were dipped into DPBS 3 times. Then, 1 ml of fixation solution, 4% Paraformaldehyde (PFA), was added. The treated samples were incubated in the dark, at room temperature for 30 min. After that, PFA was aspirated and washing steps were followed. Washing with 0.3M Glycine and double washing with DPBS were performed for 3 minutes on a shaker at 50 rpm, each. Then, the samples were incubated with a blocking solution (3% BSA) for 1 hour at 50 rpm. Primary antibodies, MBP (Abcam, Cat. No. ab62631) and MOG (Santa-Cruz, Cat. No. sc-166172) were directly added to the blocking solution with optimized dilution factors (1:750 and 1:100, respectively). Incubation took place for 16 hours at 4 ^{0}C. Following that, the samples were washed with DPBS three times. Either goat anti-rabbit IgG Alexa Fluor 488 (for MBP) or 647 (for MOG) (Invitrogen, Cat. No. A11008 and Abcam, Cat.No. ab150119, respectively.) was added onto solutions with a dilution factor of 1:1000, and incubated for 3 hours at RT. The samples were washed 3 times with DPBS and stained either with Antifade Mounting Medium with DAPI (VECTASHIELD®, Cat. No. H-1200-10) (for 2D) or incubated with Hoechst (Thermo Scientific, Cat. No. 62249) (1:1000) (for 3D) for 5 min. Imaging was performed with Leica- DMI8 SP8 confocal microscopy.

2.13 2D treatment with UV and GelMA

A separate treatment of UV and GelMA was applied to HOG cells cultured in a 2D environment. 80 x 10^3 HOG cells each were seeded onto 3 different wells of a 6 well plate(Considering 4 mn/ml condition was used to assess expression levels in 3D; 20 µl x 4 mn/ml = 80 x 10^3). After incubation for a day, their media were aspirated. Then, the treatment with either UV for 50 seconds from 50 mm above or with 20 µl GelMA was performed. One of the wells was not treated, serving as a control group. Then the fresh medium was added, and RNA isolation was conducted on the second day after treatment using the same protocol for 2D cultured HOG cells.

2.14 Coculture of SH-SY5Y and HOG cells

Once the singular optimization of HOG and SH-SY5Y cells within GelMA was attained, the co-coculture studies were initiated. The expression of Red Fluorescent Protein (RFP) by SH-SY5Y and Green Fluorescent Protein (GFP) by HOG cells was accomplished, allowing distinctive labelling while monitoring their physiological interactions. When combined with GelMA, the final cell densities for RFP-tagged SH-SY5Y and GFP-tagged HOG cells were 1 mn/ml and 4 mn/ml, respectively. Such determination of cell densities was due to individual optimization of the cells (See Sections 3.2 - 3.3, and 3.10 – 3.11). Encapsulation was mediated for 40 sec and 50 sec. The images were taken on day 0, day 3, day 5, and day 7. The constructs were consecutively washed with DPBS and the culture medium. The culture medium comprised a combination of 1X DMEM F12 and 4X DMEM High Glucose in both experimental setups. The media were changed every other day.

2.15 Statistical Analysis

Prism software (v.8; GraphPad Software, San Diego, CA, United States) was used for statistical analyses and graph generation. Significance levels were set at a confidence interval of 5%. Sample variation was quantified as the standard error of the mean (SEM), unless stated otherwise.

Chapter 3:
RESULTS

3.1 Increased duration of UV exposure results in smaller pore sizes

The quantification of pore sizes in differentially crosslinked GelMA constructs revealed the inverse proportion between UV exposure duration and the size of pores (Figure 3.1a). A statistically significant difference in average pore size according to exposure duration was found ($F(2) = 9.226$, $p = 0.0001$). Average pore sizes in constructs exposed to UV for 30 seconds and 40 seconds were 26.20 μm and 22.07 μm, respectively. 50 seconds of duration led to the average pore size of 15.82 μm, which is remarkably different from of 30- and 40-sec ($p<0.0001$, and $p<0.0001$, respectively). The images taken illustrated the roughly sizes. The pores were randomly distributed with distinct sizes (Figure 3.1b)

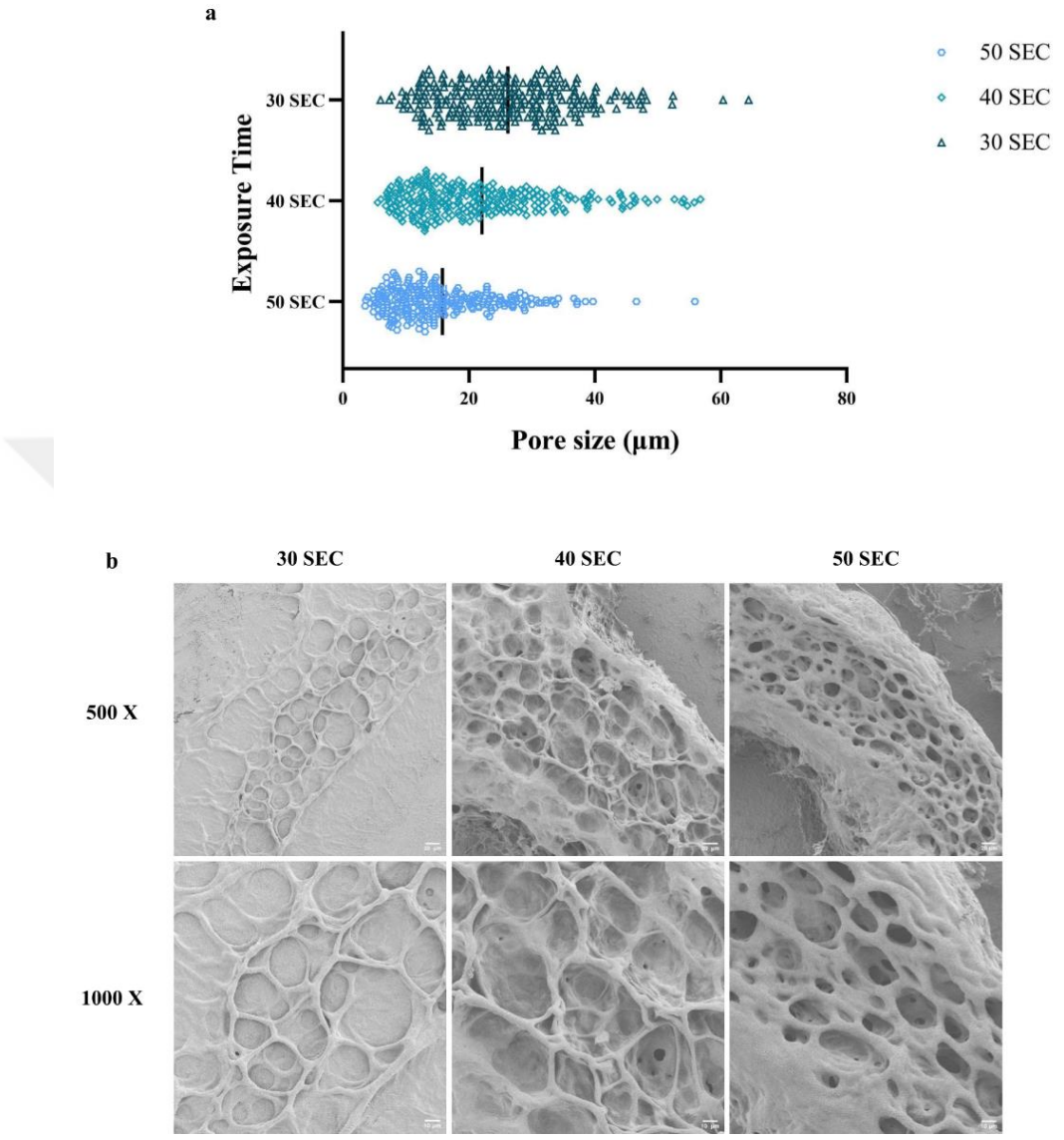

Figure 3.1. The comparative effect of UV exposure duration on GelMA pore size. a) Inverse relation between UV exposure duration and the size of pores was present. b) SEM imaging illustrated the roughly sizes of pores, which were heterogeneously distributed. Scale bars: 20 µm and 10 µm, with magnifications 500 X and 1000 X, respectively.

3.2 Viability of HOG cells is positively correlated with initial cell density

The effect of initial encapsulated cell densities (1 mn/ml, 2 mn/ml, 4 mn/ml) on the viability of HOG cells was tested over 5 days. The UV exposure duration was set to 40 seconds considering the previous observations on other tested cell lines in our research group (unpublished data). The viability of HOG cells was induced with increased cell density, indicating the importance of initial number of encapsulated cells in survival (Figure 3.2). There was a significant difference between 1 mn/ml, and 2 mn/ml, and 4 mn/ml ($p=0.018$ and $p=0.028$, respectively). Viable cell density at day 5 did not significantly differ in 4 mn/ml compared to 2 mn/ml ($p=0.97$), in fact, the mean values were close to each other (562.48% and 583.63% respectively).

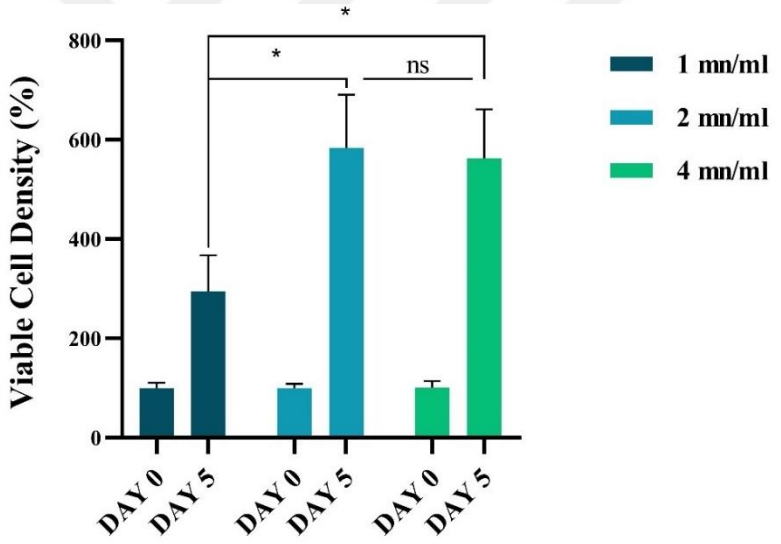

*Figure 3.2. The effect of initial cell density on the viability of HOG cells at day 5. The percentage of viable cell densities was normalized to day 0 individually. ANOVA test is based on duplicates in four independent experiments (n = 4). p-values: * < 0.05. Margin of error: SEM.*

3.3 Viability of HOG cells is enhanced by UV exposure duration

The effect of UV exposure duration on viability was tested over a 5-day period. The initial cell density was set at 4 mn/ml, although no significant viability difference was observed compared to 2 mn/ml. The selection of 4 mn/ml aims to optimize conditions for the upcoming RNA isolation experiments, focusing on maximizing RNA yield. The

viability of cells followed a rising pattern with greater UV exposure time from 40-sec on; the difference between the conditions of 30-sec and 40-sec was insignificant (viability % mean difference: 9.58, p=0.99) (Figure 3.3). Viable cell percentage at day 5 was found be significantly greater in 50 seconds of duration (710.9), compared to both 30- (538.5) and 40- sec (528.9) (p=0.036 and p=0.027, respectively). These results may imply the effect of stiffness dynamics appearing from distinct crosslinking durations, as further discussed in detail (See Discussion).

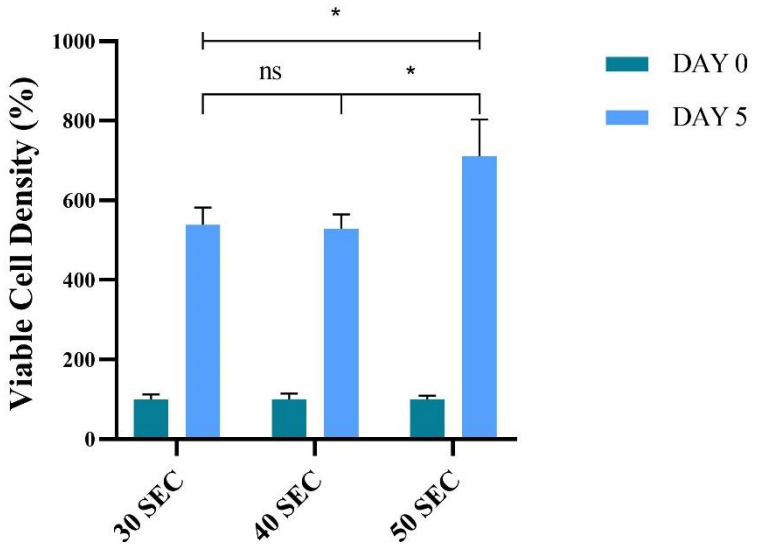

*Figure 3.3. The effect of UV exposure duration on the viability of HOG cells at day 5. The percentage of viable cell densities was normalized to day 0 individually. ANOVA test is based on duplicates in four independent experiments (n = 4). p-values: * < 0.05. Margin of error: SEM.*

3.4 The Formation of HOG Spheroids is favored via UV Exposure and Duration of Incubation

The behavior of HOG cells tended toward spheroid formation when encapsulation was maintained with a greater duration of UV exposure. The formation of spheroids was observed on day 5 under UV exposure conditions of 40 and 50 seconds, with the latter duration showing a notable effect, at 4 mn/ml cell density (p= 0.008) (Figure 3.4a). On the other hand, in the 30-sec condition, a discernable amount of cell aggregates was detected on day 5 yet no spheroids were deemed present. The mean diameter of cell aggregates in the given condition was 45.08 μm, significantly lower than that of 50-sec (mean difference: 10.67 μm, p=0.005). Between the conditions of 30- and 40-sec, the

mean difference in cell aggregate/spheroid sizes was 3.29 μm, p=0.479). For 40- and 50-sec, mean diameters were 48.37 and 55.75 μm, respectively (Figure 3.4b). The number of cell aggregates per mm^2 was favored via increased UV exposure duration. In the condition of 50-sec, the mean number was 101.2/mm^2, significantly greater from of 30- and 40-sec (30.18 and 83.01/mm^2, $p<0.0001$ and $p=0.002$, respectively) (Figure 3.4c).

Building upon the aforementioned data, an assessment of the dynamics of spheroid formation over time was conducted for the condition of 50-sec. The individual appearance of cells on day 0 was rapidly diminished by day 3 and replaced by the formation of cell aggregates, and spheroids (Figure 3.4d). On day 7, single cell population was found to be minor, accompanied by an increased number of spheroids with larger volumes. The mean size of spheroids on day 7 was 63.06 μm, significantly greater than on day 3 (14.64 ± 2.563 μm, $p<0.0001$) (Figure 3.4). Spheroid accumulation predominantly occurred along the outer edges of the constructs on both days (Figure 3.4f and Figure 3.4g) ($p< 0.0001$ both). The mean diameter of the outer aggregates on day 7 was significantly greater than of day 3, 77.63 μm and 56.39 μm, respectively (-21.24 ± 4.162, $p < 0.0001$).

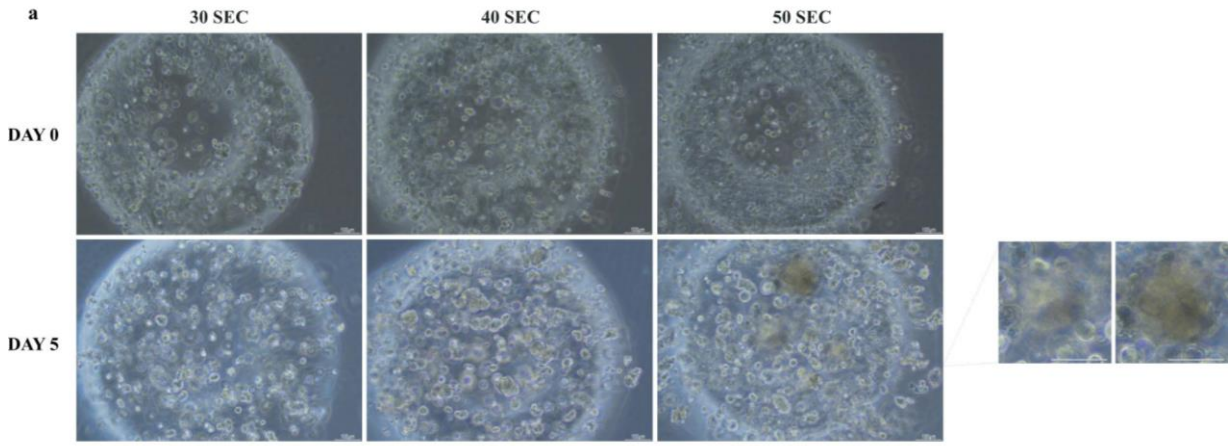
a
30 SEC
40 SEC
50 SEC
DAY 0
DAY 5

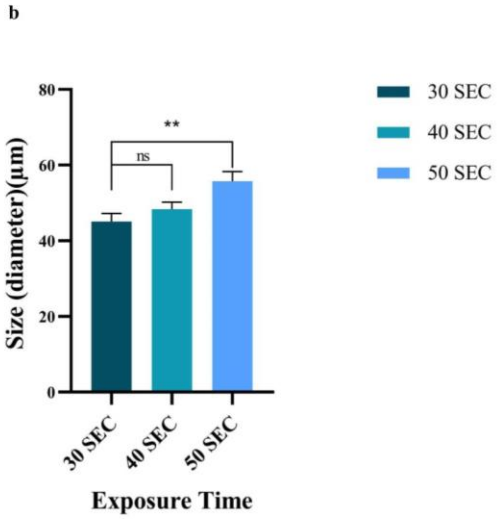
b
Size (diameter)(µm)
80
60
40
20
0
**
ns
30 SEC
40 SEC
50 SEC
Exposure Time

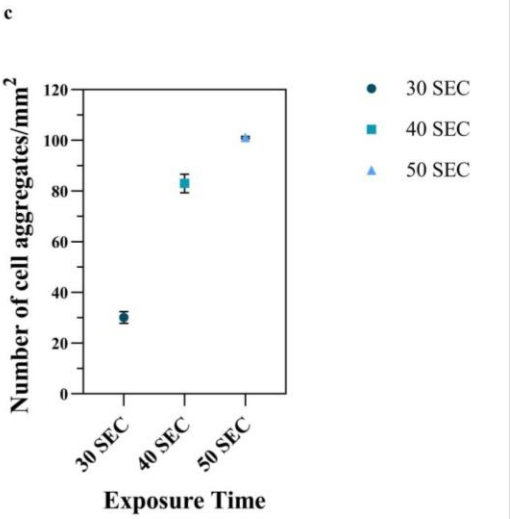
c
Number of cell aggregates/mm2
120
100
80
60
40
20
0
30 SEC
40 SEC
50 SEC
Exposure Time

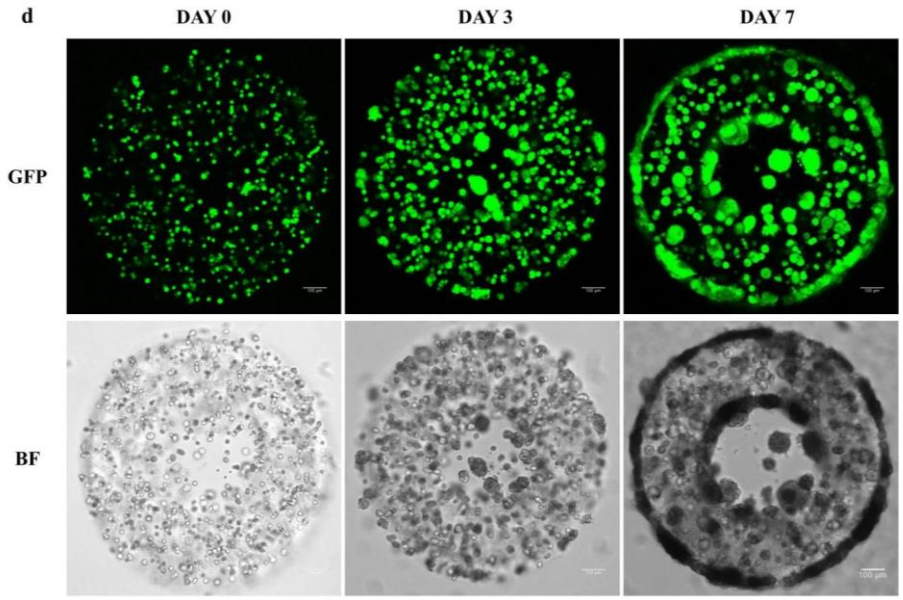
d
DAY 0
DAY 3
DAY 7
GFP
BF

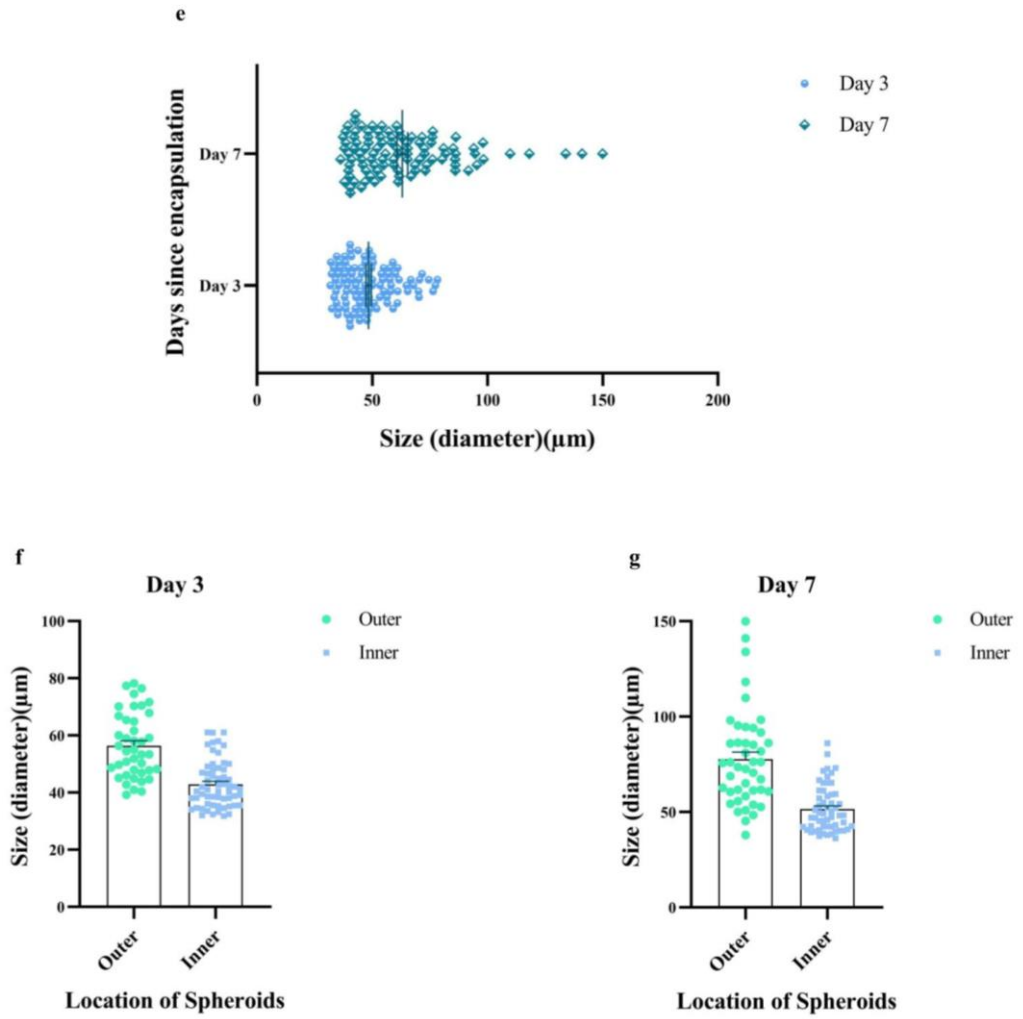

Figure 3.4. The comparative effect of UV and incubation duration on the behavior of HOG cells. Encapsulation of HOG cells with a density of 4 million per ml within 5% GelMA. Crosslinking is mediated for 30, 40, and 50 sec, from the distance of 50 mm (above). Scale bar: 100 µm. a) The formation of spheroids was observed on day 5 under UV exposure conditions of 40 and 50 seconds, with the latter duration showing a notable effect, at 4mn/ml cell density. b) The mean diameter of cell aggregates is greater in more crosslinked conditions. c) The number of cell aggregates per mm^2 is the highest in 50-sec. d) In the condition of 50 seconds of exposure, the formation of cell aggregates, and spheroids is enhanced by day. e) At day 7, rise in the mean diameters of cell aggregates/spheroids is observed. f) and g) Accumulation of spheroid along the outer edges of the constructs on both days.

3.5 Maintenance in GelMA upregulates OPC and OL markers, and rescues HOG cells from astrocyte lineage

Following GelMA maintenance of HOG cells (4 mn/ml) with 50 seconds of exposure, mRNA expression of transcription factors OLIG2 ($p = 0.002$), SOX2 ($p = 0.0036$) and SOX10 ($p=0.032$)(Figure 3.5a), OPC markers PDGFRα ($p = 0.009$) and NG2 ($p = 0.234$) (Figure 3.5b), of myOL markers MBP ($p = 0.003$) and CNPase ($p = 0.018$), and of myOL marker MOG ($p = 0.001$) (Figure 3.5c) was increased compared to of 2D maintained HOG cells. The expression of GFAP was not detected in 3D whereas it was found to be traceably expressed in 2D with a mean dCT value of 20.86 (SD=2.03) (Figure 3.5d).

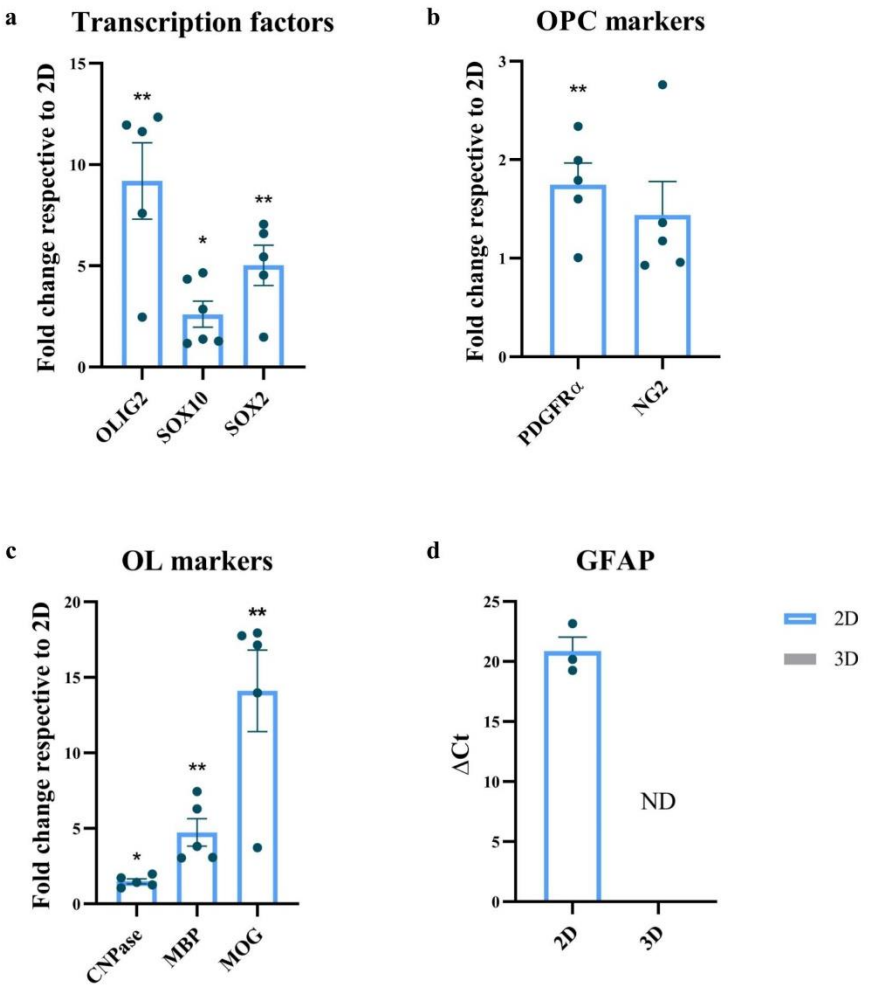

Figure 3.5. Normalized mRNA expression of the genes involved in oligodendrogenesis in GelMA maintained HOG cells. a) The expression of main regulatory transcriptions factors of OL lineage specification and b) OPC markers are

*induced in response to incubation in GelMA hydrogel. c) Increase in the expression of OL markers in HOG cells. d) Absence (Non-detection) of GFAP in 3D obtained HOG cells. OL: oligodendrocyte lineage, OPC: oligodendrocyte precursor, ND: Non detected. t-tests are based on duplicates in at least three independent experiments (n > 3). p-values: * < 0.05, ** < 0.01*

3.6 Translational expression of MOG is persistent in both 2D and 3D

The presence of MOG expression was confirmed at the protein level by immunocytochemistry in both 2D and 3D (Figure 3.6a). In 3D-maintained cells, the cells preserved their circular morphology, appearing as if they were 'enveloped' with MOG protein (Figure 3.6b). A minor number of cells was not stained with MOG in 3D condition, which may indicate some of the HOG cells exhibiting OPC features as mRNA expression of both NG2 (even though this one was not significant) and PDGFRα was found to be increased (See Section 3.5). The 3D projection of MOG signal, showcasing embedded cells, is demonstrated through confocal microscopy (Figure 3.6c).

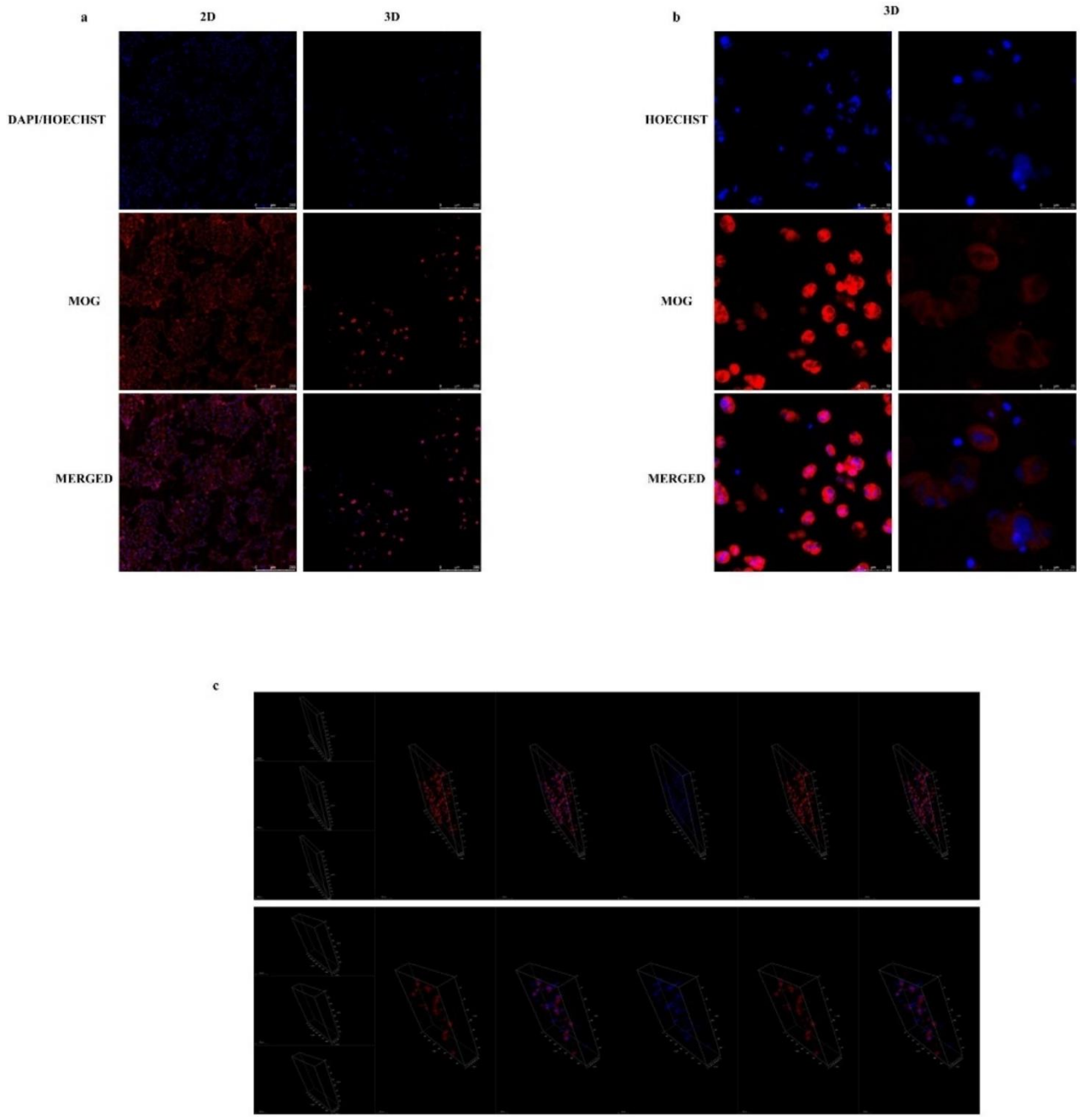

Figure 3.6. Immunocytochemical analysis of MOG in 2D cultivated and 3D maintained HOG cells. a) Representative image of MOG stainings in HOG cells in 2D versus 3D. b) Representative images of MOG presence in GelMA-maintained HOG cells with different magnifications. c) 3D projection of MOG signals.

3.7 Translational expression of MBP is persistent in both 2D and 3D

The presence of MBP expression was confirmed at the protein level by immunocytochemistry in both 2D and 3D (Figure 3.7a). Like MOG staining images, in 3D-maintained cells, the cells were observed with their circular morphology, appearing as if they were 'enveloped' with MBP protein (Figure 3.7b). Again, consistent with MOG appearance, a minor number of cells was not stained with MBP in 3D condition, which may indicate some of the HOG cells exhibiting OPC features explaining mRNA expression of both NG2 (non-significant) and PDGFRα (significant) was found to be increased (See Section 3.5). The 3D projection of MBP signal, showcasing embedded cells, is demonstrated through confocal microscopy (Figure 3.7c).

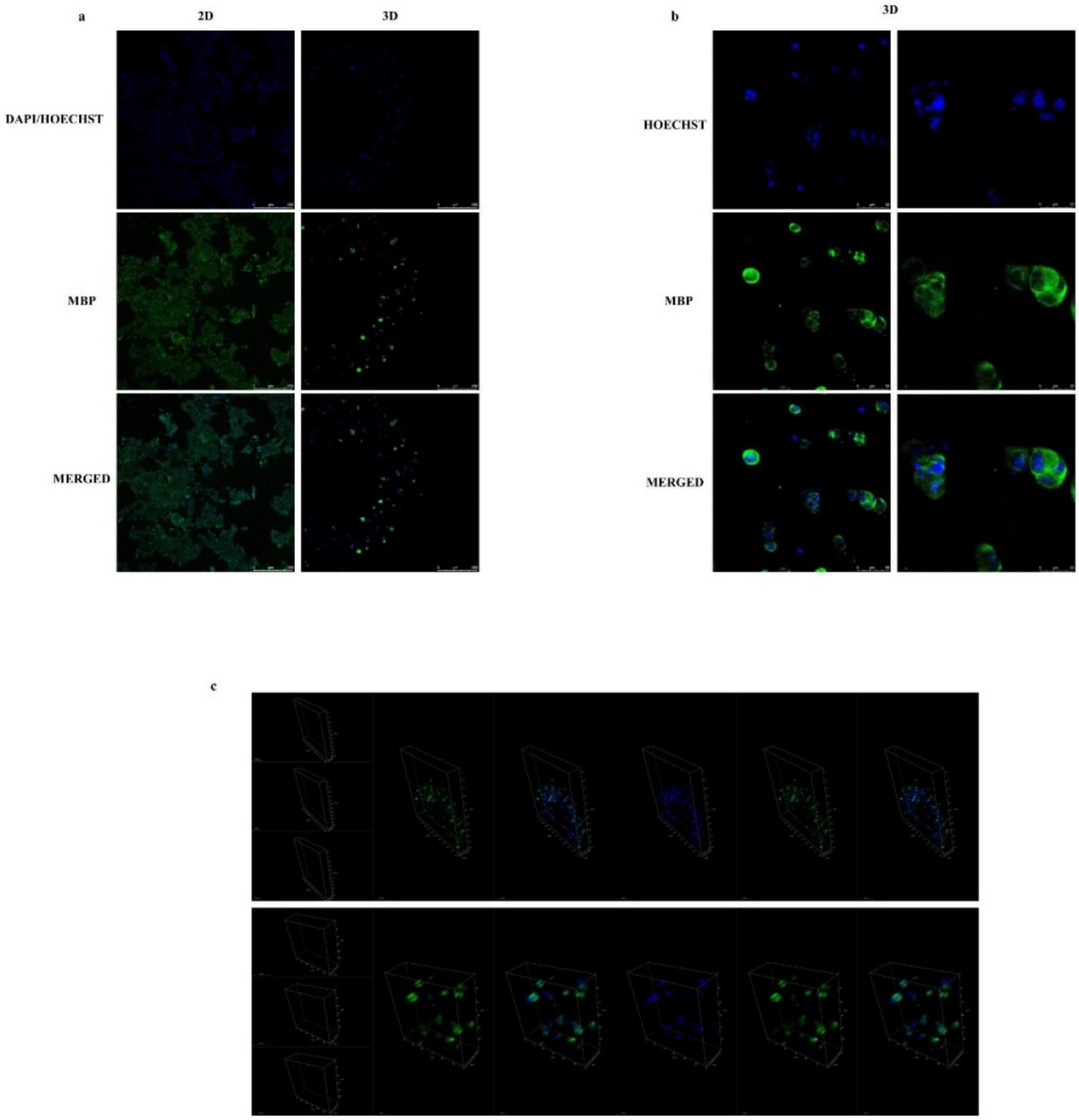

Figure 3.7. Immunocytochemical analysis of MBP in 2D cultivated and 3D maintained HOG cells. a) Representative image of MBP stainings in HOG cells in 2D versus 3D. b) Representative images of MBP presence in GelMA-maintained HOG cells with different magnifications. c) 3D projection of MBP signal.

3.8 Separate treatment of UV and GelMA in 2D condition does not significantly alter the OL expression profile of HOG cells

A separate treatment of UV and GelMA was applied to HOG cells cultured in a 2D environment. Then, the resulting impact on gene expression was compared with that of non-treated HOG cells. Neither UV treatment nor GelMA addition made significant changes in the transcriptional profile of HOG cells (Figure 3.8). In UV-exposed cells, the fold change of expressions compared to 2D were as follows: MBP: 1.18, p= 0.88; CNPase: 1.21, p= 0.47; MOG: 1.73, p= 0.56; PDGFRα: 1.69, p= 0.47; SOX10: 1.39, p= 0.56; OLIG2: 0.98, p= 0.88; NG2: 0.84, p= 0.16). The fold changes in GelMA treated cells were: MBP: 1.43, p= 0.23; CNPase: 1.20, p= 0.61; MOG: 1.17, p= 0.66; PDGFRα: 2.02, p= 0.65; SOX10: 1.39, p= 1.08; OLIG2: 0.99, p= 0.98; NG2: 0.76, p= 0.25).

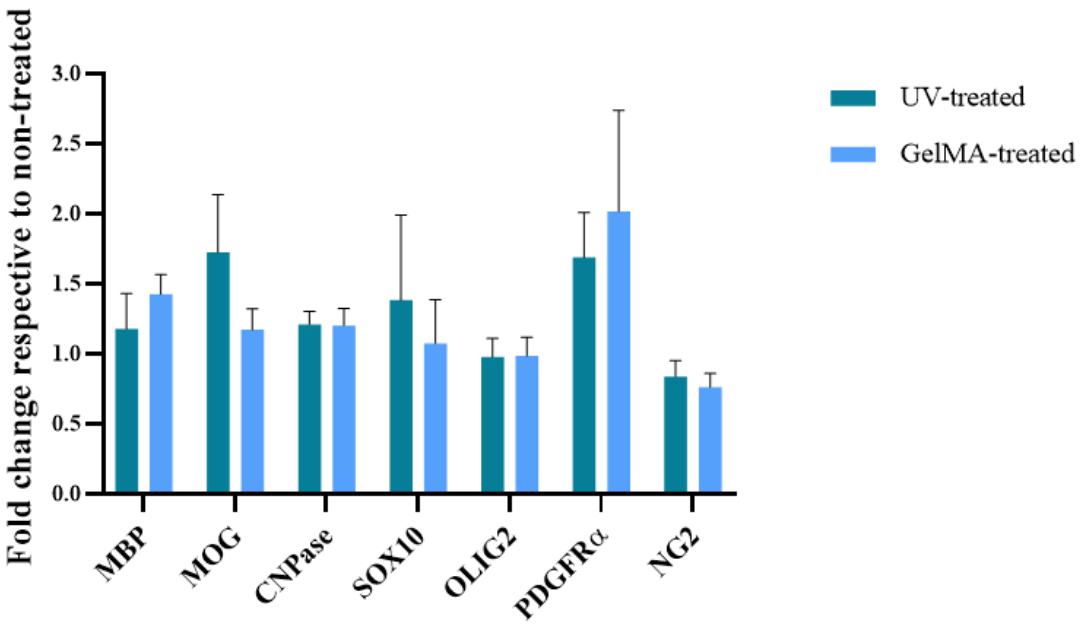

Figure 3.8. The comparison of the HOG expression profile in UV versus GelMA treated cells. The fold change values were normalized to non-treated control group. Multiple t-tests are based on triplicates in three independent experiments (n = 3). Margin of error: SEM.

3.9 UV treatment of 2D HOG cells exhibit apoptotic characteristics

The difference in morphologies between non-treated (Figure 3.9a.), GelMA treated (3.9b) and UV treated (Figure 3.9c) HOG cells was tracked for 2 days following attachment of the cells (DAY 0). At Day 1, both non treated and GelMA treated groups exhibited healthy branching, while some cells in the UV-treated group failed in this sense. At day 2, GelMA treated cells were observed to be higher in density even it was a minor difference. However, it would be inappropriate to make definitive claims since no cyto-viability assay was conducted. UV-treated cells started to display more branching by compared to their day 1, however, apoptotic cells were also present.

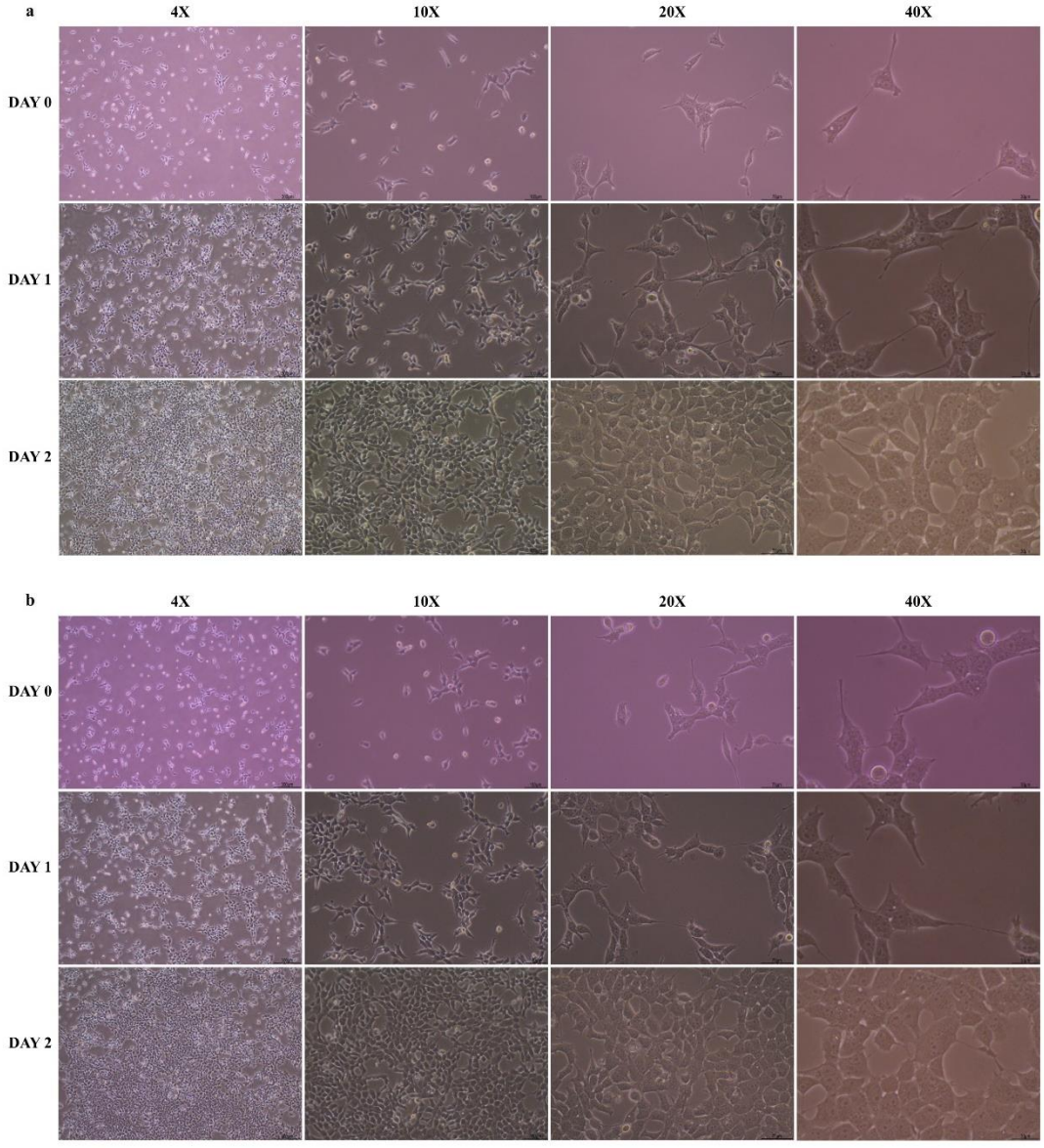

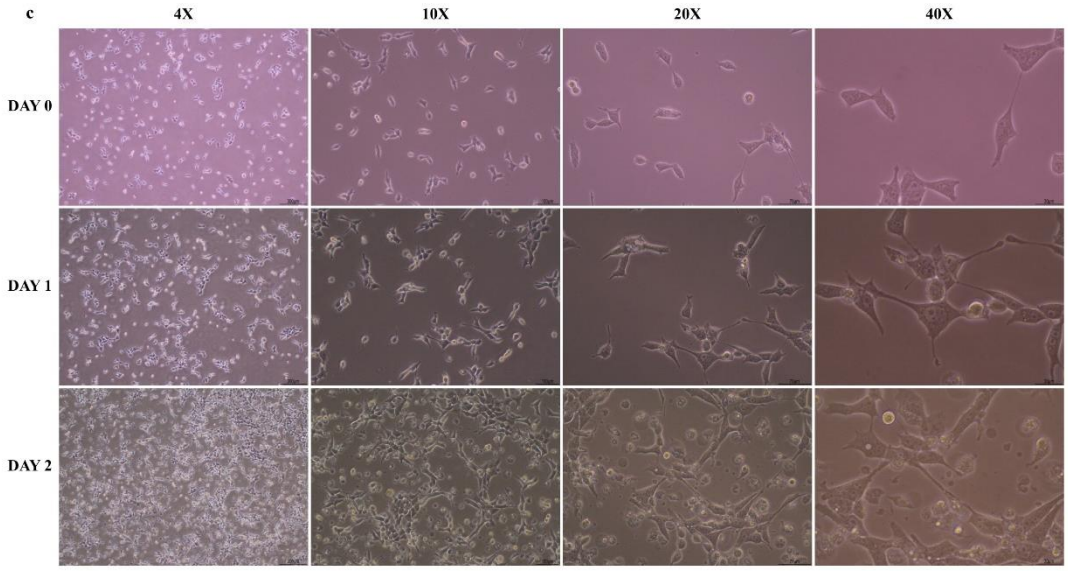

Figure 3.9. The difference in morphologies between non-treated, GelMA-treated, and UV-treated 2D HOG cells. Both non-treated (a) and GelMA-treated (b) groups exhibited healthier branching than UV-treated cells (c). At day 2, the number of cells was deemed to be greatest in GelMA- treated group. UV-treated cells started to display more branching by compared to their day 1, however, the appearance of more apoptotic cells was discerned.

3.10 The degradation of GelMA is induced with initial SH-SY5Y cell density

SH-SY5Y cells with different initial encapsulation cell densities (0.5 mn/ml, 1 mn/ml, and 1.5 mn/ml) were exposed to UV for 40 seconds. The migration of them between micropatterns and their degradation capabilities was imaged at day 0 (encapsulation day), 5 and 7 (Figure 3.10). Compared to day 0, no distinguished degradation difference was detected between the groups on day 5. Nonetheless, cells with initial density of 1.5 mn/ml displayed higher features of migrations, which could be accredited increased cell number. On day 7 groups with 1 mn/ml and 1.5 mn/ml exhibited complete degradation of the hydrogel, again; can be related to higher cell density.

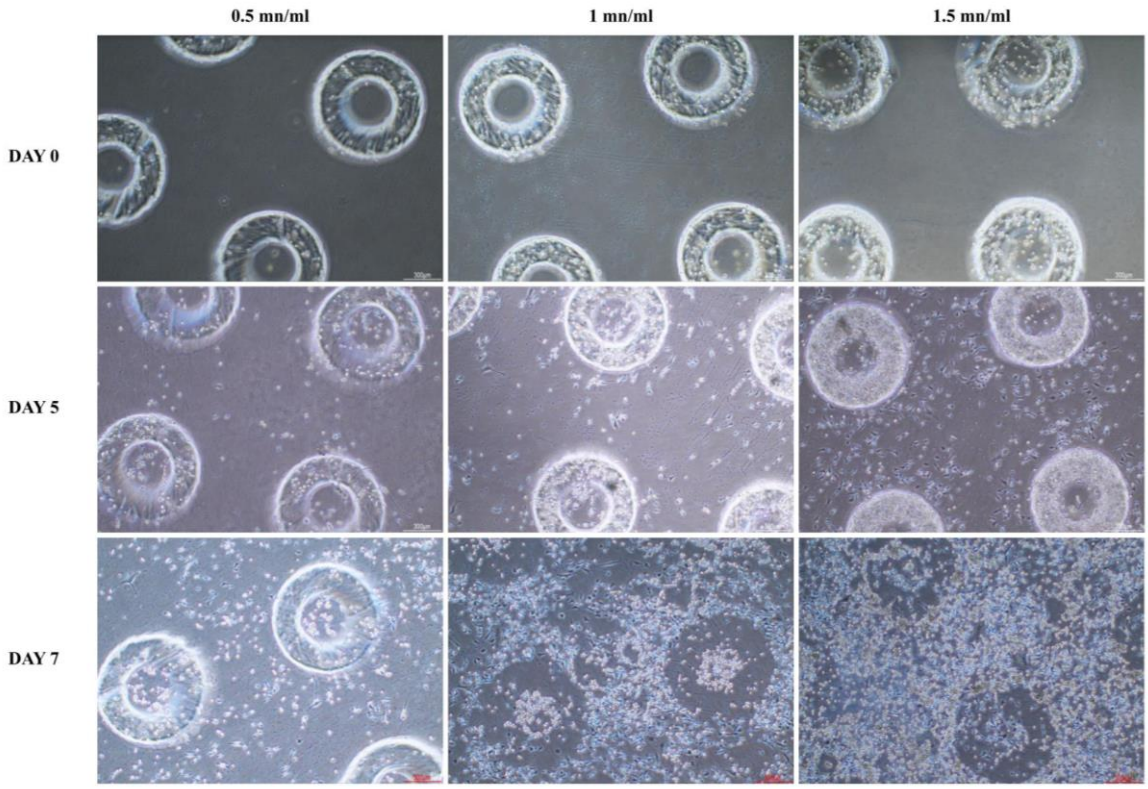

Figure 3.10. The effect of initial cell densities on the degradation of GelMA and migration of SH-SY5Y cells. While the conditions of 1 mn/ml and 1.5 mn/ml had displayed the most remarkable changes accompanied with complete degradation on day 7 respective to day 0. There was not an obvious difference in 0.5 mn/ml. Scale bar: 300 µm.

3.11 Viability of SH-SY5Y is reduced with increased UV exposure

The effect of UV exposure duration on the viability of SH-SY5Y (1 mn/ml) cells was tested over a 5-day period. The viability of cells followed a reducing pattern with greater UV exposure time from 40-sec to 60-sec ($p=0.001$); the mean viability percentages on day 5 were as follows: 40-sec: 684.2; 50-sec: 459.3; 60-sec: 279.5 (Figure 3.11a). Viable cell percentage at day 5, was found be significantly lower in 60 sec of duration compared to both 40- and 50-sec ($p<0.0001$ and $p=0.003$, respectively). The degradation of GelMA and migration of SH-SY5Y cells was facilitated in 40-sec condition (Figure 3.11b).

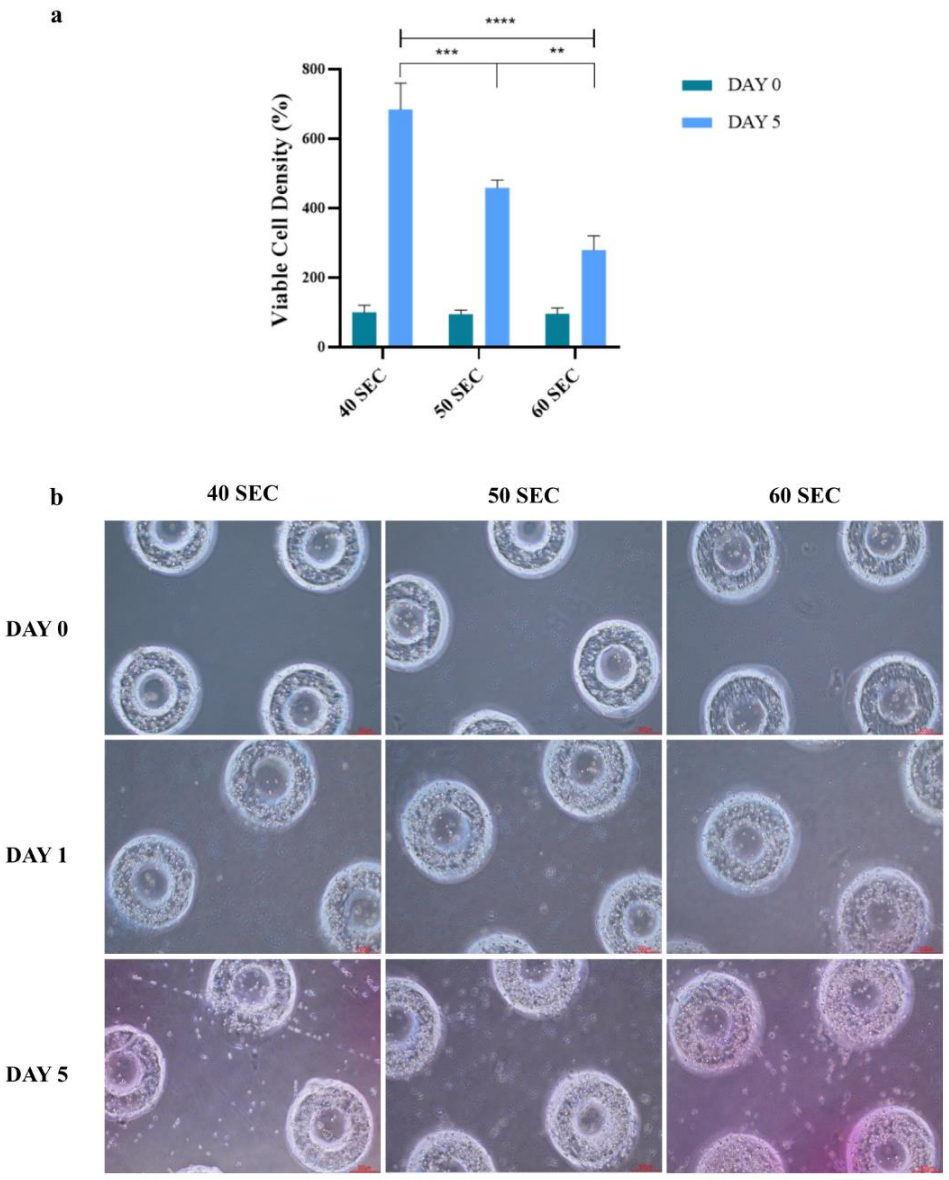

*Figure 3.11. The effect of UV exposure duration on the viability and migration of SH-SY5Y cells. a) Inverse relation between UV exposure duration and SH-SY5Y proliferation. The percentage of viable cell densities was normalized to day 0 individually. ANOVA test is based on duplicates in four independent experiments (n = 4). p-values: ** < 0.05, *** < 0.001, **** < 0.0001 b) Microscopy imaging illustrated that the degradation of GelMA and migration of SH-SY5Y cells was more pronounced in 40-sec condition. Scale bar: 300 μm. Margin of error: SEM*

3.12 SH-SY5Y branching is present in all UV exposure conditions

Even though UV exposure duration had adverse effect on the viability of SH-SY5Y cells, morphological features of it was observed to be similar in all the crosslinking conditions in which the branching was discern (Figure 3.12). At day 1, the SH-SY5Y cells started to exhibit their extensions.

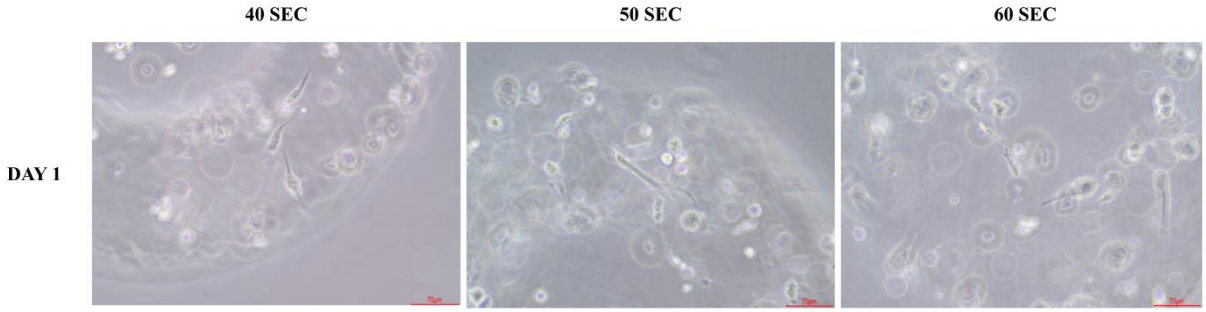

Figure 3.12. SH-SY5Y branching in different UV exposure conditions (40 sec, 50 sec, and 60 sec) illustrates that morphological characteristics are similar in all those conditions. Scale bar: 70 µm

3.13 Viability of SH-SY5Y follows a positive trend over 7 days

After optimization of the encapsulation conditions (1 mn/ml, 50-sec) for SH-SY5Y cells, MTT analysis over 7-day period was conducted. Such optimization was decided since the degradation of GelMA occurred earlier than expected and was persistent in the conditions of 1 mn/ml and 1.5 mn/ml when the UV exposure time was set to 40 seconds. 0.5 mn/ml was not selected for further studies since healthy cellular features seemed not to be sufficient.

There was no significant viability difference between day 0 and day 1 (mean difference: 45.4%, p=0.4). On day 4 and day 7 viable cell percentage was significantly greater respective to day 0 (462.9% and 691.3%, respectively; $p < 0.0001$ for both) (Figure 3.13).

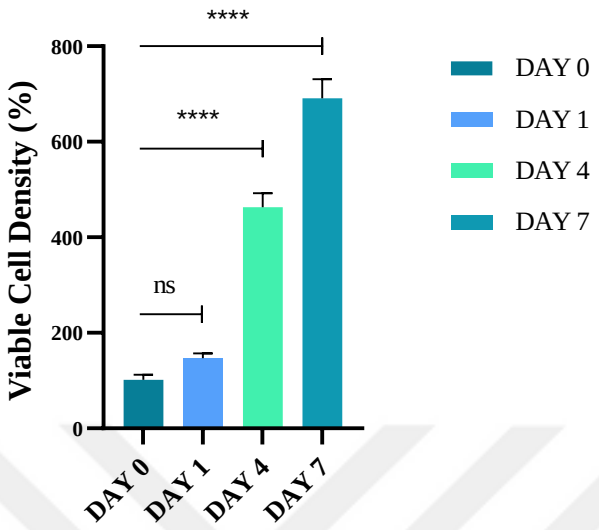

*Figure 3.13. Viability of SH-SY5Y cells over 7 days. Viability of SH-SY5Y cells (1 mn/ml) that were encapsulated with the conditions of 50-sec of UV exposure from 50 mm above. The percentage of viable cell densities was normalized to day 0 individually. ANOVA test is based on duplicates in four independent experiments (n = 4). p-values: **** < 0. 0001.Margin of error: SEM*

3.14 The interaction between SH-SY5Y and HOG cells is facilitated within a more UV-exposed condition

To observe the interaction between SH-SY5Y and HOG cells, 3D coculture was employed, where the initial encapsulation densities of them were 1 mn/ml and 4 mn/ml, respectively. The cell density of both SH-SY5Y and HOG cells was observed to be increasing day by day with longer UV exposure time (Figure 3.14a). Distinctive images illustrating their individual occupancy were taken on day 5 with confocal microscopy (Figure 3.14b). Merged images revealed the accumulation of SH-SY5Y cells proximal to HOG cell aggregates at 40-sec condition (Figure 3.14c), with a more pronounced rise at 50-sec near HOG spheroids (Figure 3.14d). The 3D projection showcasing the interactions on day 5, is demonstrated through confocal microscopy (Figure 3.14e and Figure 3.14f).

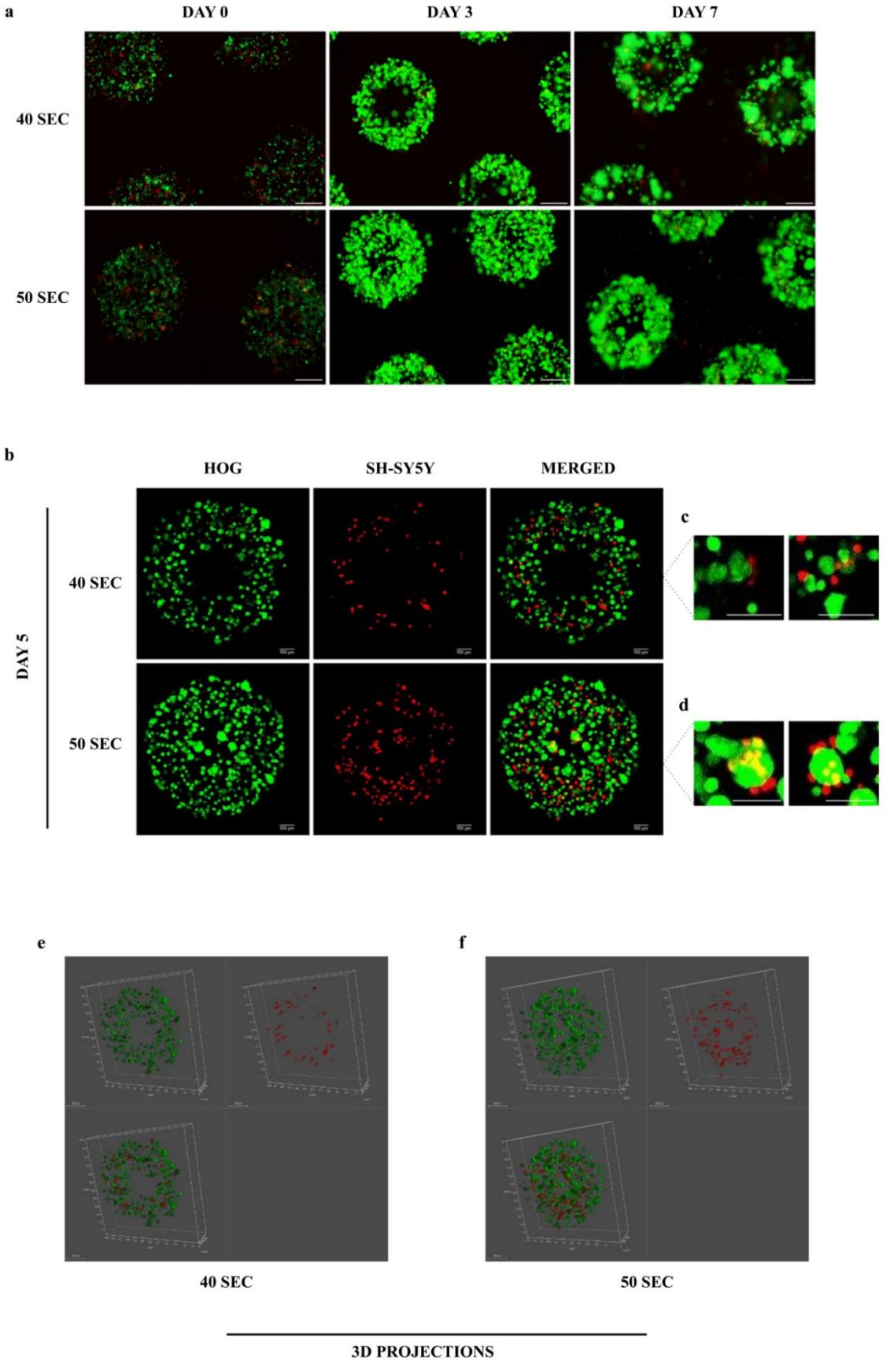
a
DAY 0
DAY 3
DAY 7
40 SEC
50 SEC
b
HOG
SH-SY5Y
MERGED
DAY 5
40 SEC
50 SEC
c
d
e
f
40 SEC
50 SEC
3D PROJECTIONS

Figure 3.14. The 3D-3D interaction between SH-SY5Y (RFP, red) and HOG (GFP, green) cells. SH-SY5Y (1 mn/ml) and HOG (4 mn/ml) cells are concurrently encapsulated for 40 or 50 seconds. a) The density of both cells was deemed higher with increased UV. Scale bar: 300 µm. b) The accumulation of SH-SY5Y cells near HOG aggregates and spheroids at day 5 (c and d), with later exposure duration, 50-sec, showing a notable effect (d) Scale bar: 100 µm. e) 3D projection of SH-SY5Y - HOG interaction on day 5, at 40-sec condition. f) 3D projection of SH-SY5Y - HOG interaction on day 5, at 50-sec condition. Scale bar: 200 µm.

Chapter 4:
DISCUSSION

Despite accumulating efforts being put into elucidating the mechanisms of oligodendrogenesis in vivo, there persists a need for in vitro platforms serving as suitable models. Here, a multiplexed and micropatterned 3D GelMA hydrogel was generated to investigate the fate of HOG cells within. Both viability and spheroid formation dynamics were codependent on prolonged UV exposure durations. This finding was unanticipated considering the well-known detrimental effect of UV radiation (Sharifi et al., 2021). One plausible factor leading such increase could be the preference of HOG cells for a stiffer environment. This assumption is grounded in the idea that increased UV exposure time (30 to 50 seconds) had a direct impact on the stiffness of GelMA hydrogel. Adjusting the UV curation dose and time is recognized as integral aspects for tuning hydrogel mechanical properties, including stiffness (Xiao et al., 2019). Earlier research demonstrated that elastic modulus of GelMA hydrogel becomes larger with the increase of UV exposure time. O'Connell et al. (2018) observed a parallel relationship between the slope of the stiffness gradient and the UV exposure time of the 10% GelMA solution, up to approximately 70 seconds. Another study, utilizing the same UV equipment and employing the same GelMA concentration as herein, reported the photopolymerization onset of 5% GelMA to be 15 seconds, accompanied by an increased elastic modulus (E) within a range of 15 to 120 seconds (Lin et al., 2013). SEM images here demonstrated an inverse relation between pore sizes and UV exposure duration. Kim et al. (2020) shown that stiffer GelMA hydrogels have smaller pore size. Collectively, one could argue that an exposure time of 50 seconds resulted in an environment characterized by the highest stiffness in this study. The moduli of the 3D culture conditions, 30, 40, and 50 seconds of UV durations, must yet to be determined. Noteworthy, these results emphasize the importance of ECM characteristics in shaping cell behavior with which similar studies are in agreement. For instance, CG4 cells, the cells reflecting the main features of OPCs, in a hyaluronic acid-gelatin matrix displayed round morphology in cell aggregates within stiffer hydrogel, aligning with this study's observations (Li et al., 2013). Notably, Li et al. (2013) observed that more spherical morphology was emerging as the storage modulus (E') increased, starting from 120 Pa and trending towards 1000 Pa.

The proliferation rate was found to be greater when E'<120 Pa, whereas maintenance in stiffer conditions (E'>120) led to the opposite. Conversely, here the proliferation of HOG cells was the greatest in 50-sec condition, indicating a direct proportional relation between stiffness and viability. Leipzig and Shoichet (2009) revealed distinguished proliferation and differentiation patterns of Neuronal stem cells (NSCs) on MAC (methacyrlamide chitosan) surfaces with different stiffness values: <1 kPa, 3.5 kPa, and 7 kPa. The number of oligodendrocytes was greater at 7 kPa which indicates oligodendrocytes proliferation was induced with increased stiffness. When the stiffness was <1 kPa, the expressions of MOG and CNPase were the highest, suggesting that the maturation of oligodendrocytes is enhanced in less stiff hydrogels.

In contrary to above, Russell and Lampe (2017) demonstrated that proliferation and larger spheroid formation of MADM cells were deemed in a more compliant PEG-based scaffold. Unal and colleagues reported likewise in MADM cells within hyaluronic acid-based hydrogels (Unal et al., 2020). Unfortunately, since storage modulus values for the tested conditions with distinct UV exposures were not measured, it remains elusive at which kPa values HOG cells display these monitored features. Variety in these results, including here, may have arisen from the difference in source materials, cells, and even culturing conditions.

Regarding spheroid formation by HOG cells, it should be noted that this study not only demonstrated the effect of UV duration but also the potential correlation of spheroid accumulation on the outer edges of micropatterned gels (See *Figure 3.4*). Facile diffusion of medium components on the proximity may have been the reason for increased number and size of spheroids along the edges.

The impact of UV exposure duration was scrutinized in SH-SY5Y cells as well. Contradictory to HOG cells, the viability of SH-SY5Y cells was inversely affected in response to UV exposure. This may be due to the toxic effect of UV or/and change in stiffness. Coculture of SH-SY5Y cells with HOG cells was conducted to understand if an interaction would occur. Although SH-SY5Y cells were not differentiated into mature neurons, their interaction with HOG cells was evident, leading to accumulation near HOG spheroids with the latter crosslinking exhibiting a notable effect.

This finding holds promise for further exploration involving mature neurons and oligodendrocyte lineage cells within the hydrogel to unravel the model's potential for accurately representing myelination processes as well.

Another important factor determining the characteristics of HOG cells in GelMA was the initial cell densities, consistent with the previous studies of oligodendroglial cells in vitro (De Kleijn et al., 2019; Janowska et al., 2018). Given that, although there was no significant viability difference at day 5 between 2 mn/ml and 4 mn/ml, experiments have proceeded with 4 mn/ml to assess differential mRNA and protein expressions compared to 2D cultivated cells. That was because of the major concern of RNA yield: isolation from the 4 mn/ml condition had yielded more RNA concentration (unpublished data). Maintenance in GelMA induced the expression of transcription factors OLIG2, SOX2, and SOX10, pointing to the initiation of early oligodendrocyte development. However, considering the controversy about the role of SOX2 in literature, it would be erroneous to be confidently argued. Notwithstanding that SOX2 is known for its function in maintaining an undifferentiated precursor state (Shen et al., 2008; Graham et al., 2003), its activator role in OL differentiation has been acknowledged (Hoffmann et al., 2014; Zhang et al., 2018). In so much that Zhang et al. (2018) recommended SOX2 as a therapeutic target for dysmyelinating and demyelinating disorders.

It has been shown that OLIG2 is a primary determinant of oligodendrocyte fate specification (Liu et al., 2007; Dai et al., 2015). Based on the findings of this thesis and previously mentioned observations in the literature, the increased expression of PDGFRα and myelination markers MBP and MOG demonstrated here may be ascribed to the synergistic effect of OLIG2 and SOX families. A direct correlation between OLIG2 and SOX2 was reported in recent studies, underlying these observations. Domingo-Muelas et al. (2023) found that SOX2 and OLIG2 expressions positively correlate since SOX2 can bind to the regulatory region of OLIG2. Another study demonstrated that, following the OLIG2 knockdown, a substantial decrease occurred in the expression of SOX2 (Kupp et al., 2016). Likewise, OLIG2 silencing was shown to lead to the downregulation of PDGFRα, bearably indicating commensurate relation. Deficiency of SOX10 has been found to exert similar effects (Finzch et al., 2008). One of the earliest studies regarding the role of SOX10 established that the terminal differentiation of myelin-forming oligodendrocytes depends on the activity of SOX10 (Stolt et al., 2002). Both SOX2 and SOX10 are able to bind to the promoter region of the MBP gene (Hoffman et al. 2014;

Wei et al., 2004; Stolt et al., 2002) which may be one of the possible explanations for the transcriptional upregulation of MBP in findings here. Likewise, studies on mice and zebrafish highlighted the cooperation between OLIG families and SOX10 in the upregulation of MBP (Wissmuller et al., 2006; Li et al., 2007), which again could be one of the ongoing upregulatory mechanisms within 3D-HOG cells even after the expression profile of OLIG1 was not tested. MOG has been recently identified as a target of SOX8 and SOX10. Turnescu et al. (2018) showed that transcription of MOG was downregulated in SOX8 deficient mice, and its downregulation was further accelerated upon deletion of SOX10. Hence, like the increased MBP transcription in 3D-HOG cells, MOG upregulation may also be pursued to SOX10.

At the immunocytochemical level, the expression of MBP together with MOG was persistent in 2D and 3D maintained cells. The exact quantitative comparison was not given, conduction of western blotting may be considered for further. A minor number of cells was not stained with MOG and MBP in 3D condition, which may indicate some of the HOG cells exhibiting OPC features as mRNA expression of both NG2, even it was not significant, and PDGFRα was found to be increased. In 2D context, discrepancies in findings exist where the expression of MBP was reported to be either present (Buntinx et al., 2003, Post and Dawson, 1992) or lacking (Arriba Zerpa et al., 2000; Dkleijn et al., 2019) in differentiated HOG cells. Furthermore, it has been suggested that HOG cells may not completely represent oligodendroglia characteristics since the expression of astrocyte markers, including GFAP, is detected even after HOG cells are maintained in various media that supposedly should induce oligodendrocyte differentiation (Dkleijn et al., 2019). Here, the absence of GFAP in cells obtained from GelMA conditions may indicate a possible rescue of HOG cells from the astrocyte lineage. As a potential explanation, OLIG2-mediated regulation of the lineage specification of NG2 cells may be exemplified based on the previous findings. For instance, Zhu et al. (2012) stated that in the neocortex and corpus callosum of transgenic mice, and the neocortex of perinatal mice, NG2 cells differentiated into astrocytes instead of oligodendrocytes when OLIG2 was deleted. In parallel, deletion of OLIG2 in immature astrocytes caused GFAP upregulation occurred in the cortex (Cai et al., 2007). Hence, it can be interpreted that HOG cells expressing higher levels of OLIG2 compared to 2D-maintained cells are more likely to possess oligodendrocyte characteristics rather than astrocyte. On the other hand, Komitova et al. (2011) investigated the OLIG2 knockout in NG2 cells around a stab

wound and concluded that differentiation into astroglial cells did not occur. It was claimed that OLIG2 is not an important regulator of NG2 cells in the neocortex of adult mice.

In support of the observed effect of GelMA on HOG cells, the injection of GelMA hydrogel into SCI mice models resulted in the downregulation of GFAP (Zhang and Saijilafu, 2021). Even not in the context of CNS, Shahidi et al. (2021) found increased expression of MBP and MAG in Schwann cells and enhanced myelination via GelMA maintenance in comparison with incubation on Poly-d Lysine (PDL) and collagen. Overall, these evidence suggest the positive regulatory role of the GelMA in oligodendrogenesis and myelination both in CNS and peripheral nervous system (PNS).

To ascertain whether alterations in the expression of OL genes were exclusive to 3D maintenance, a separate treatment of UV and GelMA was applied to HOG cells cultured in a 2D environment. Then, the resulting impact on gene expression was compared with that of non-treated HOG cells. Expectedly, neither UV treatment nor GelMA addition made significant changes on the expression profile of HOG cells. Thus, it can be more confidently reinforced that 3D maintenance has a unique and impactful role in determining the fate of HOG cells.

This study shows the regulatory effect of the GelMA environment on transcription of HOG cells. Upregulation of key transcription factors involved in OL specification (OLIG2, SOX2, and SOX10), OPC (PDGFRα and NG2), and oligodendrocyte markers (CNPase, MBP and MOG), coupled with the absence of GFAP may imply that HOG cells are committed towards OPC and OL differentiation, with a possible rescue from astrocyte lineage.

Some limitations of this study must be acknowledged. The exact quantification of the storage modulus of the constructs at different UV duration conditions needs to be performed by rheological measurements. It must be enlightened whether the stiffness of the optimized condition (4mn/ml, 50 seconds of exposure) that favors more viability and spheroid formation does match with brain tissue (200−2000 Pa (Li et al., 2012)) or with the best condition for OL maturation and myelination (<1kPa (Leipzig and Shoichet, 2009). Also, the comparison of various UV exposure durations in the context of transcriptional regulation may be considered to clarify the influence of biomaterial properties on OL specification. Notwithstanding such elusiveness, these results imply the regulatory effect of the GelMA environment on transcription, altering the fate of HOG

cells. Therefore, this platform could potentially be of note as a culture model of oligodendrogenesis.

As a further perspective, co-culture of HOG cells with neurons may be considered to assess the potency of myelination utilizing this model. Additionally, the 3D GelMA hydrogel model may offer two main contributions to drug development studies. First, it may serve as a bridging platform between 2D and in vivo myelination studies thanks to its biomimetic properties. Second, it holds the potential to be employed in CNS drug-delivering studies owing to its biodegradability and biocompatibility.

Chapter 5:
CONCLUSION

The study unfolds the impact of a multiplexed and micropatterned 3D GelMA platform on the cellular behavior and expression profile of HOG cells. Both proliferation and spheroid formation were enhanced with prolonged crosslinking durations, illustrating the importance of ECM dynamics on cellular behavior. This study shows the regulatory effect of the GelMA environment on transcription of HOG cells. Upregulation of key transcription factors involved in OL specification (OLIG2, SOX2, and SOX10), OPC (PDGFRα and NG2), and oligodendrocyte markers (CNPase, MBP and MOG), coupled with the absence of GFAP may imply that HOG cells are committed towards OPC and OL differentiation, with a possible rescue from astrocyte lineage. Neither UV treatment nor GelMA addition in 2D had significant changes on the expression profile of HOG cells, suggesting the exclusiveness of 3D. The introduction of a coculture experiment with SH-SY5Y cells provided an additional layer to the study, revealing interactions near HOG spheroids, particularly notable with prolonged crosslinking. However, the non-differentiation of SH-SY5Y cells into mature neurons must be acknowledged. The conclusion suggests the need for further exploration involving mature neurons and oligodendrocyte lineage cells within the hydrogel to unravel the model's potential for accurately representing myelination processes as well.

BIBLIOGRAPHY

Aboul-Enein, F., Rauschka, H., Kornek, B., Stadelmann, C., Stefferl, A., Brück, W., Lucchinetti, C., Schmidbauer, M., Jellinger, K., & Lassmann, H. (2003). Preferential loss of myelin-associated glycoprotein reflects hypoxia-like white matter damage in stroke and inflammatory brain diseases. *Journal of neuropathology and experimental neurology, 62*(1), 25–33. https://doi.org/10.1093/jnen/62.1.25

Ahmed E. M. (2015). Hydrogel: Preparation, characterization, and applications: A review. *Journal of advanced research, 6*(2), 105–121. https://doi.org/10.1016/j.jare.2013.07.006

Akay, L., Effenberger, A., & Tsai, L. (2021). Cell of all trades: oligodendrocyte precursor cells in synaptic, vascular, and immune function. *Genes &Amp; Development, 35*(3-4), 180-198. doi: 10.1101/gad.344218.120

de Arriba Zerpa, G. A., Saleh, M. C., Fernández, P. M., Guillou, F., Espinosa de los Monteros, A., de Vellis, J., Zakin, M. M., & Baron, B. (2000). Alternative splicing prevents transferrin secretion during differentiation of a human oligodendrocyte cell line. *Journal of neuroscience research, 61*(4), 388–395. https://doi.org/10.1002/1097-4547(20000815)61:4<388::AID-JNR5>3.0.CO;2-Q

Bakhti, M., Aggarwal, S., & Simons, M. (2014). Myelin architecture: zippering membranes tightly together. *Cellular and molecular life sciences : CMLS, 71*(7), 1265–1277. https://doi.org/10.1007/s00018-013-1492-0

Baumann, N., & Pham-Dinh, D. (2001). Biology of oligodendrocyte and myelin in the mammalian central nervous system. *Physiological reviews, 81*(2), 871–927. https://doi.org/10.1152/physrev.2001.81.2.871

Bello-Morales, R., Crespillo, A. J., Fraile-Ramos, A., Tabarés, E., Alcina, A., & López-Guerrero, J. A. (2012). Role of the small GTPase Rab27a during herpes simplex virus infection of oligodendrocytic cells. *BMC microbiology, 12*, 265. https://doi.org/10.1186/1471-2180-12-265

Benarroch, E. (2015). Extracellular matrix in the CNS. *Neurology*, *85*(16), 1417-1427. doi: 10.1212/wnl.0000000000002044

Bergles, D., & Richardson, W. (2015). Oligodendrocyte Development and Plasticity. *Cold Spring Harbor Perspectives In Biology*, *8*(2), a020453. doi: 10.1101/cshperspect.a020453

Bugiani, M., Postma, N., Polder, E., Dieleman, N., Scheffer, P. G., Sim, F. J., van der Knaap, M. S., & Boor, I. (2013). Hyaluronan accumulation and arrested oligodendrocyte progenitor maturation in vanishing white matter disease. *Brain : a journal of neurology*, *136*(Pt 1), 209–222. https://doi.org/10.1093/brain/aws320

Buntinx, M., Vanderlocht, J., Hellings, N., Vandenabeele, F., Lambrichts, I., Raus, J., Ameloot, M., Stinissen, P., & Steels, P. (2003). Characterization of three human oligodendroglial cell lines as a model to study oligodendrocyte injury: morphology and oligodendrocyte-specific gene expression. *Journal of neurocytology*, *32*(1), 25–38. https://doi.org/10.1023/a:1027324230923

Buntinx, M., Moreels, M., Vandenabeele, F., Lambrichts, I., Raus, J., Steels, P., Stinissen, P., & Ameloot, M. (2004). Cytokine-induced cell death in human oligodendroglial cell lines: I. Synergistic effects of IFN-gamma and TNF-alpha on apoptosis. *Journal of neuroscience research*, *76*(6), 834–845. https://doi.org/10.1002/jnr.20118

Cai, J., Chen, Y., Cai, W. H., Hurlock, E. C., Wu, H., Kernie, S. G., Parada, L. F., & Lu, Q. R. (2007). A crucial role for Olig2 in white matter astrocyte development. Development *(Cambridge, England)*, *134*(10), 1887–1899. https://doi.org/10.1242/dev.02847

Clarke, L. E., Young, K. M., Hamilton, N. B., Li, H., Richardson, W. D., & Attwell, D. (2012). Properties and fate of oligodendrocyte progenitor cells in the corpus callosum, motor cortex, and piriform cortex of the mouse. *The Journal of neuroscience: the official journal of the Society for Neuroscience*, *32*(24), 8173–8185. https://doi.org/10.1523/JNEUROSCI.0928-12.2012

Cramer, M., & Badylak, S. (2019). Extracellular Matrix-Based Biomaterials and Their Influence Upon Cell Behavior. Annals Of Biomedical Engineering, 48(7), 2132-2153. doi: 10.1007/s10439-019-02408-9

Couttas, T. A., Kain, N., Suchowerska, A. K., Quek, L. E., Turner, N., Fath, T., Garner, B., & Don, A. S. (2016). Loss of ceramide synthase 2 activity, necessary for myelin biosynthesis, precedes tau pathology in the cortical pathogenesis of Alzheimer's disease. *Neurobiology of aging*, *43*, 89–100. https://doi.org/10.1016/j.neurobiolaging.2016.03.027

Dai, J., Bercury, K. K., Ahrendsen, J. T., & Macklin, W. B. (2015). Olig1 function is required for oligodendrocyte differentiation in the mouse brain. *The Journal of neuroscience: the official journal of the Society for Neuroscience*, *35*(10), 4386–4402. https://doi.org/10.1523/JNEUROSCI.4962-14.2015

De Kleijn, K., Zuure, W., Peijnenborg, J., Heuvelmans, J., & Martens, G. (2019). Reappraisal of Human HOG and MO3.13 Cell Lines as a Model to Study Oligodendrocyte Functioning. *Cells*, *8*(9), 1096. doi: 10.3390/cells8091096

Dimou, L., & Gallo, V. (2015). NG2-glia and their functions in the central nervous system. *Glia*, *63*(8), 1429–1451. https://doi.org/10.1002/glia.22859

Domingo-Muelas, A., Morante-Redolat, J. M., Moncho-Amor, V., Jordán-Pla, A., Pérez-Villalba, A., Carrillo-Barberà, P., Belenguer, G., Porlan, E., Kirstein, M., Bachs, O., Ferrón, S. R., Lovell-Badge, R., & Fariñas, I. (2023). The rates of adult neurogenesis and oligodendrogenesis are linked to cell cycle regulation through p27-dependent gene repression of SOX2. *Cellular and molecular life sciences: CMLS*, *80*(1), 36. https://doi.org/10.1007/s00018-022-04676-6

Donati, D. (2020). Viral infections and multiple sclerosis. *Drug Discovery Today: Disease Models*, *32*, 27-33. doi: 10.1016/j.ddmod.2020.02.003

Duncan, I. D., & Radcliff, A. B. (2016). Inherited and acquired disorders of myelin: The underlying myelin pathology. *Experimental neurology*, *283*(Pt B), 452–475. https://doi.org/10.1016/j.expneurol.2016.04.002

Ersoy, F., & Sokullu, E. (2019). A compartmental 3D scaffold fabrication and alignment device for neurovascular co-culture and tri-culture. *Biomedical Physics & Engineering Express*, *5*(3), 035034. https://doi.org/10.1088/2057-1976/ab0dcc

Fan, Y., Avci, N. G., Nguyen, D. T., Dragomir, A., Akay, Y. M., Xu, F., & Akay, M. (2015). Engineering a High-Throughput 3-D In Vitro Glioblastoma Model. *IEEE journal of translational engineering in health and medicine, 3*, 4300108. https://doi.org/10.1109/JTEHM.2015.2410277

Fields, R. D., & Dutta, D. J. (2019). Treadmilling Model for Plasticity of the Myelin Sheath. *Trends in neurosciences, 42*(7), 443–447. https://doi.org/10.1016/j.tins.2019.04.002

Finzsch, M., Stolt, C. C., Lommes, P., & Wegner, M. (2008). Sox9 and Sox10 influence survival and migration of oligodendrocyte precursors in the spinal cord by regulating PDGF receptor alpha expression. *Development (Cambridge, England), 135*(4), 637–646. https://doi.org/10.1242/dev.010454

Fletcher, J. L., Makowiecki, K., Cullen, C. L., & Young, K. M. (2021). Oligodendrogenesis and myelination regulate cortical development, plasticity and circuit function. *Seminars in cell & developmental biology, 118*, 14–23. https://doi.org/10.1016/j.semcdb.2021.03.017

Franco-Pons, N., Virgos, C., Vogel, W. F., Ureña, J. M., Soriano, E., del Rio, J. A., & Vilella, E. (2006). Expression of discoidin domain receptor 1 during mouse brain development follows the progress of myelination. *Neuroscience, 140*(2), 463–475. https://doi.org/10.1016/j.neuroscience.2006.02.033

Graham, V., Khudyakov, J., Ellis, P., & Pevny, L. (2003). SOX2 functions to maintain neural progenitor identity. *Neuron, 39*(5), 749–765. https://doi.org/10.1016/s0896-6273(03)00497-5

Greer, J. M., & Lees, M. B. (2002). Myelin proteolipid protein--the first 50 years. *The international journal of biochemistry & cell biology, 34*(3), 211–215. https://doi.org/10.1016/s1357-2725(01)00136-4

Gomez-Pinedo, U., Matías-Guiu, J., Torre-Fuentes, L., Montero-Escribano, P., Hernández-Lorenzo, L., & Pytel, V. et al. (2022). Variant rs4149584 (R92Q) of the TNFRSF1A gene in patients with familial multiple sclerosis. *Neurología (English Edition)*. doi: 10.1016/j.nrleng.2022.07.002

Haase, S., Haghikia, A., Gold, R., & Linker, R. A. (2018). Dietary fatty acids and susceptibility to multiple sclerosis. *Multiple sclerosis (Houndmills, Basingstoke, England)*, *24*(1), 12–16.

Hobson, G. M., & Garbern, J. Y. (2012). Pelizaeus-Merzbacher disease, Pelizaeus-Merzbacher-like disease 1, and related hypomyelinating disorders. *Seminars in neurology*, *32*(1), 62–67. https://doi.org/10.1055/s-0032-1306388

Hodes, M. E., Pratt, V. M., & Dlouhy, S. R. (1993). Genetics of Pelizaeus-Merzbacher disease. *Developmental neuroscience*, *15*(6), 383–394. https://doi.org/10.1159/000111361

Hoffmann, S. A., Hos, D., Küspert, M., Lang, R. A., Lovell-Badge, R., Wegner, M., & Reiprich, S. (2014). Stem cell factor Sox2 and its close relative Sox3 have differentiation functions in oligodendrocytes. *Development (Cambridge, England)*, *141*(1), 39–50. https://doi.org/10.1242/dev.098418

Janowska, J., Ziemka-Nalecz, M., & Sypecka, J. (2018). The Differentiation of Rat Oligodendroglial Cells Is Highly Influenced by the Oxygen Tension: In Vitro Model Mimicking Physiologically Normoxic Conditions. *International journal of molecular sciences*, *19*(2), 331. https://doi.org/10.3390/ijms19020331

Kang, S. H., Li, Y., Fukaya, M., Lorenzini, I., Cleveland, D. W., Ostrow, L. W., Rothstein, J. D., & Bergles, D. E. (2013). Degeneration and impaired regeneration of gray matter oligodendrocytes in amyotrophic lateral sclerosis. *Nature neuroscience*, *16*(5), 571–579. https://doi.org/10.1038/nn.3357

Kim, C., Young, J. L., Holle, A. W., Jeong, K., Major, L. G., Jeong, J. H., Aman, Z. M., Han, D. W., Hwang, Y., Spatz, J. P., & Choi, Y. S. (2020). Stem Cell Mechanosensation on Gelatin Methacryloyl (GelMA) Stiffness Gradient Hydrogels. *Annals of biomedical engineering*, *48*(2), 893–902. https://doi.org/10.1007/s10439-019-02428-5

Kitagawa, K., Sinoway, M. P., Yang, C., Gould, R. M., & Colman, D. R. (1993). A proteolipid protein gene family: expression in sharks and rays and possible evolution from an ancestral gene encoding a pore-forming polypeptide. *Neuron*, *11*(3), 433–448. https://doi.org/10.1016/0896-6273(93)90148-k

Kister, A., & Kister, I. (2023). Overview of myelin, major myelin lipids, and myelin-associated proteins. *Frontiers in chemistry*, *10*, 1041961. https://doi.org/10.3389/fchem.2022.1041961

Komitova, M., Serwanski, D. R., Richard Lu, Q., & Nishiyama, A. (2011). *Glia*, *59*(5), 800–809. doi:10.1002/glia.21152

Kondo, T., & Raff, M. (2004). Chromatin remodeling and histone modification in the conversion of oligodendrocyte precursors to neural stem cells. *Genes & development*, *18(*23), 2963–2972. https://doi.org/10.1101/gad.309404

Kupp, R., Shtayer, L., Tien, A. C., Szeto, E., Sanai, N., Rowitch, D. H., & Mehta, S. (2016). Lineage-Restricted OLIG2-RTK Signaling Governs the Molecular Subtype of Glioma Stem-like Cells. *Cell reports*, *16*(11), 2838–2845. https://doi.org/10.1016/j.celrep.2016.08.040

Lappe-Siefke, C., Goebbels, S., Gravel, M., Nicksch, E., Lee, J., Braun, P. E., Griffiths, I. R., & Nave, K. A. (2003). Disruption of Cnp1 uncouples oligodendroglial functions in axonal support and myelination. *Nature genetics*, *33*(3), 366–374. https://doi.org/10.1038/ng1095

Lee, J., Gravel, M., Zhang, R., Thibault, P., & Braun, P. E. (2005). Process outgrowth in oligodendrocytes is mediated by CNP, a novel microtubule assembly myelin protein. *The Journal of cell biology*, *170*(4), 661–673. https://doi.org/10.1083/jcb.200411047

Leipzig, N. D., & Shoichet, M. S. (2009). The effect of substrate stiffness on adult neural stem cell behavior. *Biomaterials*, *30*(36), 6867–6878. https://doi.org/10.1016/j.biomaterials.2009.09.002

Levenberg, S., Huang, N. F., Lavik, E., Rogers, A. B., Itskovitz-Eldor, J., & Langer, R. (2003). Differentiation of human embryonic stem cells on three-dimensional polymer scaffolds. *Proceedings of the National Academy of Sciences of the United States of America*, *100*(22), 12741–12746. https://doi.org/10.1073/pnas.1735463100

Li, H., Lu, Y., Smith, H. K., & Richardson, W. D. (2007). Olig1 and Sox10 interact synergistically to drive myelin basic protein transcription in oligodendrocytes. *The Journal of neuroscience : the official journal of the Society for Neuroscience*, *27*(52), 14375–14382. https://doi.org/10.1523/JNEUROSCI.4456-07.2007

Li, X., Katsanevakis, E., Liu, X., Zhang, N., & Wen, X. (2012). Engineering neural stem cell fates with hydrogel design for central nervous system regeneration. *Progress In Polymer Science*, *37*(8), 1105-1129. doi: 10.1016/j.progpolymsci.2012.02.004

Li, X., Liu, X., Cui, L., Brunson, C., Zhao, W., Bhat, N. R., Zhang, N., & Wen, X. (2013). Engineering an in situ crosslinkable hydrogel for enhanced remyelination. *FASEB journal: official publication of the Federation of American Societies for Experimental Biology*, *27*(3), 1127–1136. https://doi.org/10.1096/fj.12-211151

Lin, R. Z., Chen, Y. C., Moreno-Luna, R., Khademhosseini, A., & Melero-Martin, J. M. (2013). Transdermal regulation of vascular network bioengineering using a photopolymerizable methacrylated gelatin hydrogel. *Biomaterials*, *34*(28), 6785–6796. https://doi.org/10.1016/j.biomaterials.2013.05.060

Lin, S. C., & Bergles, D. E. (2004). Synaptic signaling between GABAergic interneurons and oligodendrocyte precursor cells in the hippocampus. *Nature neuroscience*, *7*(1), 24–32. https://doi.org/10.1038/nn1162

Linington, C., Bradl, M., Lassmann, H., Brunner, C., & Vass, K. (1988). Augmentation of demyelination in rat acute allergic encephalomyelitis by circulating mouse monoclonal antibodies directed against a myelin/oligodendrocyte glycoprotein. *The American journal of pathology*, *130*(3), 443–454.

Liu, Z., Hu, X., Cai, J., Liu, B., Peng, X., Wegner, M., & Qiu, M. (2007). Induction of oligodendrocyte differentiation by Olig2 and Sox10: evidence for reciprocal interactions and dosage-dependent mechanisms. *Developmental biology*, *302*(2), 683–693. https://doi.org/10.1016/j.ydbio.2006.10.007

Loessner, D., Meinert, C., Kaemmerer, E., Martine, L. C., Yue, K., Levett, P. A., Klein, T. J., Melchels, F. P., Khademhosseini, A., & Hutmacher, D. W. (2016). Functionalization, preparation and use of cell-laden gelatin methacryloyl-based hydrogels as modular tissue culture platforms. *Nature protocols*, *11*(4), 727–746. https://doi.org/10.1038/nprot.2016.037

Lossos, A., Elazar, N., Lerer, I., Schueler-Furman, O., Fellig, Y., Glick, B., Zimmerman, B. E., Azulay, H., Dotan, S., Goldberg, S., Gomori, J. M., Ponger, P., Newman, J. P., Marreed, H., Steck, A. J., Schaeren-Wiemers, N., Mor, N., Harel, M., Geiger, T., Eshed-Eisenbach, Y., … Peles, E. (2015). Myelin-associated glycoprotein gene mutation causes Pelizaeus-Merzbacher disease-like disorder. *Brain: a journal of neurology*, *138*(Pt 9), 2521–2536. https://doi.org/10.1093/brain/awv204

Love S. (2006). Demyelinating diseases. *Journal of clinical pathology, 59*(11), 1151–1159. https://doi.org/10.1136/jcp.2005.031195

Lyssiotis, C. A., Walker, J., Wu, C., Kondo, T., Schultz, P. G., & Wu, X. (2007). Inhibition of histone deacetylase activity induces developmental plasticity in oligodendrocyte precursor cells. *Proceedings of the National Academy of Sciences of the United States of America, 104*(38), 14982–14987. https://doi.org/10.1073/pnas.0707044104

Maiuolo, J., Macrì, R., Bava, I., Gliozzi, M., Musolino, V., Nucera, S., Carresi, C., Scicchitano, M., Bosco, F., Scarano, F., Palma, E., Gratteri, S., & Mollace, V. (2019). Myelin Disturbances Produced by Sub-Toxic Concentration of Heavy Metals: The Role of Oligodendrocyte Dysfunction. *International journal of molecular sciences, 20*(18), 4554.

Martini, R., & Schachner, M. (1986). Immunoelectron microscopic localization of neural cell adhesion molecules (L1, N-CAM, and MAG) and their shared carbohydrate epitope and myelin basic protein in developing sciatic nerve. *The Journal of cell biology, 103*(6 Pt 1), 2439–2448. https://doi.org/10.1083/jcb.103.6.2439

Mattei, M. G., Alliel, P. M., Dautigny, A., Passage, E., Pham-Dinh, D., Mattei, J. F., & Jollès, P. (1986). The gene encoding for the major brain proteolipid (PLP) maps on the q-22 band of the human X chromosome. *Human genetics, 72*(4), 352–353.

Martínez-Pinilla, E., Rubio-Sardón, N., Peláez, R., García-Álvarez, E., Del Valle, E., Tolivia, J., Larráyoz, I. M., & Navarro, A. (2021). Neuroprotective Effect of Apolipoprotein D in Cuprizone-Induced Cell Line Models: A Potential Therapeutic Approach for Multiple Sclerosis and Demyelinating Diseases. *International journal of molecular sciences, 22*(3), 1260. https://doi.org/10.3390/ijms22031260

Mei, R., Qiu, W., Yang, Y., Xu, S., Rao, Y., Li, Q., Luo, Y., Huang, H., Yang, A., Tao, H., Qiu, M., & Zhao, X. (2023). Evidence That DDR1 Promotes Oligodendrocyte Differentiation during Development and Myelin Repair after Injury. *International journal of molecular sciences, 24*(12), 10318. https://doi.org/10.3390/ijms241210318

Meschkat, M., Steyer, A. M., Weil, M. T., Kusch, K., Jahn, O., Piepkorn, L., Agüi-Gonzalez, P., Phan, N. T. N., Ruhwedel, T., Sadowski, B., Rizzoli, S. O., Werner, H. B., Ehrenreich, H., Nave, K. A., & Möbius, W. (2022). White matter integrity in mice requires continuous myelin synthesis at the inner tongue. *Nature communications*, *13*(1), 1163. https://doi.org/10.1038/s41467-022-28720-y

Mitew, S., Kirkcaldie, M. T., Halliday, G. M., Shepherd, C. E., Vickers, J. C., & Dickson, T. C. (2010). Focal demyelination in Alzheimer's disease and transgenic mouse models. *Acta neuropathologica*, *119*(5), 567–577. https://doi.org/10.1007/s00401-010-0657-2

Morell, P & Quarles, R.H. (1999). Characteristic composition of myelin. In: Siegel GJ, Agranoff BW, Albers RW, editors. Basic Neurochemistry: Molecular, Cellular and Medical Aspects. Lippincott-Raven

Nakano, S., Uyeda, A., Matsunaga, Y. T., & Muramatsu, R. (2023). Phenotypic and transcriptional characterization of oligodendrocyte precursor cells in a 3D culture. *Biomaterials Science*, *11*(8), 2860–2869. https://doi.org/10.1039/d2bm01897g

Nave, K. A.; Lai, C.; Bloom, F. E.; Milner, R. J. (1987). Splice site selection in the proteolipid protein (PLP) gene transcript and primary structure of the DM-20 protein of central nervous system myelin. *Proceedings of the National Academy of Sciences*, *84*(16), 5665–5669. doi:10.1073/pnas.84.16.5665

Nery, S., Wichterle, H., & Fishell, G. (2001). Sonic hedgehog contributes to oligodendrocyte specification in the mammalian forebrain. *Development (Cambridge, England)*, *128*(4), 527–540. https://doi.org/10.1242/dev.128.4.527

Nguyen, D. T., Fan, Y., Akay, Y. M., & Akay, M. (2016). Investigating Glioblastoma Angiogenesis Using A 3D in Vitro GelMA Microwell Platform. *IEEE transactions on nanobioscience*, *15*(3), 289–293. https://doi.org/10.1109/TNB.2016.2528170

O'Connell, C. D., , Zhang, B., , Onofrillo, C., , Duchi, S., , Blanchard, R., , Quigley, A., , Bourke, J., , Gambhir, S., , Kapsa, R., , Di Bella, C., , Choong, P., , & Wallace, G. G., (2018). Tailoring the mechanical properties of gelatin methacryloyl hydrogels through manipulation of the photocrosslinking conditions. *Soft matter*, *14*(11), 2142–2151. https://doi.org/10.1039/c7sm02187a

Ota, M., Sato, N., Kimura, Y., Shigemoto, Y., Kunugi, H., & Matsuda, H. (2019). Changes of Myelin Organization in Patients with Alzheimer's Disease Shown by q-Space Myelin Map Imaging. *Dementia and geriatric cognitive disorders extra*, *9*(1), 24–33. https://doi.org/10.1159/000493937

Park, J., Lim, E., Back, S., Na, H., Park, Y., & Sun, K. (2010). Nerve regeneration following spinal cord injury using matrix metalloproteinase-sensitive, hyaluronic acid-based biomimetic hydrogel scaffold containing brain-derived neurotrophic factor. *Journal of biomedical materials research. Part A*, *93*(3), 1091–1099. https://doi.org/10.1002/jbm.a.32519

Palermo, S., Lopiano, L., Morese, R., Zibetti, M., Romagnolo, A., Stanziano, M., Rizzone, M. G., Geminiani, G. C., Valentini, M. C., & Amanzio, M. (2018). Role of the Cingulate Cortex in Dyskinesias-Reduced-Self-Awareness: An fMRI Study on Parkinson's Disease Patients. *Frontiers in psychology*, *9*, 1765. https://doi.org/10.3389/fpsyg.2018.01765

Palaniyar, N., Semotok, J., Wood, D., Moscarello, M., & Harauz, G. (1998). Human proteolipid protein (PLP) mediates winding and adhesion of phospholipid membranes but prevents their fusion. *Biochimica Et Biophysica Acta (BBA) - Biomembranes*, *1415*(1), 85-100. doi: 10.1016/s0005-2736(98)00180-1

Pringle, N. P., Mudhar, H. S., Collarini, E. J., & Richardson, W. D. (1992). PDGF receptors in the rat CNS: during late neurogenesis, PDGF alpha-receptor expression appears to be restricted to glial cells of the oligodendrocyte lineage. *Development (Cambridge, England)*, *115*(2), 535–551. https://doi.org/10.1242/dev.115.2.535

Pronker, M. F., Lemstra, S., Snijder, J., Heck, A. J. R., Thies-Weesie, D. M. E., Pasterkamp, R. J., & Janssen, B. (2016). Structural basis of myelin-associated glycoprotein adhesion and signalling. *Nature Communications*, *7*(1). https://doi.org/10.1038/ncomms13584

Post, G. R., & Dawson, G. (1992). Characterization of a cell line derived from a human oligodendroglioma. *Molecular and chemical neuropathology, 16*(3), 303–317. https://doi.org/10.1007/BF03159976

Pozniak, C. D., Langseth, A. J., Dijkgraaf, G. J., Choe, Y., Werb, Z., & Pleasure, S. J. (2010). Sox10 directs neural stem cells toward the oligodendrocyte lineage by decreasing Suppressor of Fused expression. *Proceedings of the National Academy of Sciences of the United States of America, 107*(50), 21795–21800. https://doi.org/10.1073/pnas.1016485107

Qin, J., Sikkema, A. H., van der Bij, K., de Jonge, J. C., Klappe, K., Nies, V., Jonker, J. W., Kok, J. W., Hoekstra, D., & Baron, W. (2017). GD1a Overcomes Inhibition of Myelination by Fibronectin via Activation of Protein Kinase A: Implications for Multiple Sclerosis. *The Journal of neuroscience: the official journal of the Society for Neuroscience, 37*(41), 9925–9938. https://doi.org/10.1523/JNEUROSCI.0103-17.2017

Raasakka, A., & Kursula, P. (2014). The myelin membrane-associated enzyme 2',3'-cyclic nucleotide 3'-phosphodiesterase: on a highway to structure and function. *Neuroscience bulletin, 30*(6), 956–966. https://doi.org/10.1007/s12264-013-1437-5

Rowlands, D., Sugahara, K., & Kwok, J. (2015). Glycosaminoglycans and Glycomimetics in the Central Nervous System. *Molecules, 20*(3), 3527-3548. doi: 10.3390/molecules20033527

Raskind, W. H., Williams, C. A., Hudson, L. D., & Bird, T. D. (1991). Complete deletion of the proteolipid protein gene (PLP) in a family with X-linked Pelizaeus-Merzbacher disease. *American journal of human genetics, 49*(6), 1355–1360.

Relucio, J., Menezes, M. J., Miyagoe-Suzuki, Y., Takeda, S., & Colognato, H. (2012). Laminin regulates postnatal oligodendrocyte production by promoting oligodendrocyte progenitor survival in the subventricular zone. *Glia, 60*(10), 1451–1467. https://doi.org/10.1002/glia.22365

Ruskamo, S., Raasakka, A., Pedersen, J., Martel, A., Škubník, K., & Darwish, T. et al. (2022). Human myelin proteolipid protein structure and lipid bilayer stacking. *Cellular And Molecular Life Sciences, 79*(8). doi: 10.1007/s00018-022-04428-6

Russell, L., & Lampe, K. J. (2017). Oligodendrocyte Precursor Cell Viability, Proliferation, and Morphology is Dependent on Mesh Size and Storage Modulus in 3D Poly(ethylene glycol)-Based Hydrogels. *ACS Biomaterials Science & Engineering*, *3*(12),3459–3468. https://doi.org/10.1021/acsbiomaterials.7b00374

Rosso, M., & Chitnis, T. (2020). Association Between Cigarette Smoking and Multiple Sclerosis: A Review. *JAMA neurology*, *77*(2), 245–253.

Sato, T., Shirai, R., Isogai, M., Yamamoto, M., Miyamoto, Y., & Yamauchi, J. (2022). Hyaluronic acid and its receptor CD44, acting through TMEM2, inhibit morphological differentiation in oligodendroglial cells. *Biochemical and biophysical research communications*, *624*, 102–111. https://doi.org/10.1016/j.bbrc.2022.07.092

Sawyer, S. W., Oest, M. E., Margulies, B.S., Soman, S. (2016). Behavior of Encapsulated Saos-2 Cells within Gelatin Methacrylate Hydrogels. *Journal of Tissue Science and Engineering*, *7*(2). https://doi.org/10.4172/2157-7552.1000173

Schoenfeld, R., Wong, A., Silva, J., Li, M., Itoh, A., Horiuchi, M., Itoh, T., Pleasure, D., & Cortopassi, G. (2010). Oligodendroglial differentiation induces mitochondrial genes and inhibition of mitochondrial function represses oligodendroglial differentiation. *Mitochondrion*, *10*(2), 143–150. https://doi.org/10.1016/j.mito.2009.12.141

Shah, N., Hallur, P., Ganesh, R., Sonpatki, P., Naik, D., & Chandrachari, K. et al. (2021). Gelatin methacrylate hydrogels culture model for glioblastoma cells enriches for mesenchymal-like state and models interactions with immune cells. *Scientific Reports*, *11*(1). doi: 10.1038/s41598-021-97059-z

Shahidi, S., Janmaleki, M., Riaz, S., Sanati Nezhad, A., & Syed, N. (2021). A tuned gelatin methacryloyl (GelMA) hydrogel facilitates myelination of dorsal root ganglia neurons in vitro. *Materials science & engineering. C, Materials for biological applications*, *126*, 112131. https://doi.org/10.1016/j.msec.2021.112131

Sharifi, S., Sharifi, H., Akbari, A., & Chodosh, J. (2021). Systematic optimization of visible light-induced crosslinking conditions of gelatin methacryloyl (GelMA). *Scientific Reports*, *11*(1). doi: 10.1038/s41598-021-02830-x

Shen, S., Sandoval, J., Swiss, V. A., Li, J., Dupree, J., Franklin, R. J., & Casaccia-Bonnefil, P. (2008). Age-dependent epigenetic control of differentiation inhibitors is critical for remyelination efficiency. *Nature neuroscience, 11*(9), 1024–1034. https://doi.org/10.1038/nn.2172

Shirahama, H., Lee, B., Tan, L., & Cho, N. (2016). Precise Tuning of Facile One-Pot Gelatin Methacryloyl (GelMA) Synthesis. *Scientific Reports, 6*(1). doi: 10.1038/srep31036

Silva, M. E., Hernández-Andrade, M., Abasolo, N., Espinoza-Cruells, C., Mansilla, J. B., Reyes, C. R., Aranda, S., Esteban, Y., Rodriguez-Calvo, R., Martorell, L., Muntané, G., Rivera, F. J., & Vilella, E. (2023). DDR1 and Its Ligand, Collagen IV, Are Involved in In Vitro Oligodendrocyte Maturation. *International journal of molecular sciences, 24*(2), 1742. https://doi.org/10.3390/ijms24021742

Spanier, J. A., Nashold, F. E., Mayne, C. G., Nelson, C. D., & Hayes, C. E. (2015). Vitamin D and estrogen synergy in Vdr-expressing CD4(+) T cells is essential to induce Helios(+)FoxP3(+) T cells and prevent autoimmune demyelinating disease. *Journal of neuroimmunology*, *286*, 48–58. https://doi.org/10.1016/j.jneuroim.2015.06.015

Stoffel, W., Hillen, H., & Giersiefen, H. (1984). Structure and molecular arrangement of proteolipid protein of central nervous system myelin. *Proceedings of the National Academy of Sciences of the United States of America*, *81*(16), 5012–5016. https://doi.org/10.1073/pnas.81.16.5012

Stoffels, J. M., de Jonge, J. C., Stancic, M., Nomden, A., van Strien, M. E., Ma, D., Sisková, Z., Maier, O., Ffrench-Constant, C., Franklin, R. J., Hoekstra, D., Zhao, C., & Baron, W. (2013). Fibronectin aggregation in multiple sclerosis lesions impairs remyelination. *Brain: a journal of neurology, 136*(Pt 1), 116–131. https://doi.org/10.1093/brain/aws313

Stoffels, J. M., Hoekstra, D., Franklin, R. J., Baron, W., & Zhao, C. (2015). The EIIIA domain from astrocyte-derived fibronectin mediates proliferation of oligodendrocyte progenitor cells following CNS demyelination. *Glia*, *63*(2), 242–256. https://doi.org/10.1002/glia.22748

Stohlman, S. A., & Hinton, D. R. (2001). Viral induced demyelination. Brain pathology (Zurich, Switzerland), 11(1), 92–106. https://doi.org/10.1111/j.1750-3639.2001.tb00384.x

Stolt, C. C., Rehberg, S., Ader, M., Lommes, P., Riethmacher, D., Schachner, M., Bartsch, U., & Wegner, M. (2002). Terminal differentiation of myelin-forming oligodendrocytes depends on the transcription factor Sox10. *Genes & development*, *16*(2), 165–170. https://doi.org/10.1101/gad.215802

Suzuki, N., Hyodo, M., Hayashi, C., Mabuchi, Y., Sekimoto, K., Onchi, C., Sekiguchi, K., & Akazawa, C. (2019). Laminin α2, α4, and α5 Chains Positively Regulate Migration and Survival of Oligodendrocyte Precursor Cells. *Scientific Reports*, *9*(1). https://doi.org/10.1038/s41598-019-56488-7

Turnescu, T., Arter, J., Reiprich, S., Tamm, E. R., Waisman, A., & Wegner, M. (2018). Sox8 and Sox10 jointly maintain myelin gene expression in oligodendrocytes. *Glia*, *66*(2), 279–294. https://doi.org/10.1002/glia.23242

Unal, D. B., Caliari, S. R., & Lampe, K. J. (2020). 3D Hyaluronic Acid Hydrogels for Modeling Oligodendrocyte Progenitor Cell Behavior as a Function of Matrix Stiffness. *Biomacromolecules*, *21*(12), 4962–4971. https://doi.org/10.1021/acs.biomac.0c01164

Vilella, E., Gas, C., Garcia-Ruiz, B., & Rivera, F. J. (2019). Expression of DDR1 in the CNS and in myelinating oligodendrocytes. *Biochimica et biophysica acta. Molecular cell research*, *1866*(11), 118483. https://doi.org/10.1016/j.bbamcr.2019.04.010

Walton, C., King, R., Rechtman, L., Kaye, W., Leray, E., Marrie, R. A., Robertson, N., La Rocca, N., Uitdehaag, B., van der Mei, I., Wallin, M., Helme, A., Angood Napier, C., Rijke, N., & Baneke, P. (2020). Rising prevalence of multiple sclerosis worldwide: Insights from the Atlas of MS, third edition. *Multiple sclerosis (Houndmills, Basingstoke, England)*, *26*(14), 1816–1821. https://doi.org/10.1177/1352458520970841

Wajgt, A., & Górny, M. (1983). CSF antibodies to myelin basic protein and to myelin-associated glycoprotein in multiple sclerosis. Evidence of the intrathecal production of antibodies. *Acta neurologica Scandinavica*, *68*(5), 337–343. https://doi.org/10.1111/j.1600-0404.1983.tb04841.x

Warshawsky, I., Rudick, R. A., Staugaitis, S. M., & Natowicz, M. R. (2005). Primary progressive multiple sclerosis as a phenotype of a PLP1 gene mutation. *Annals of neurology*, *58*(3), 470–473. https://doi.org/10.1002/ana.20601

Wegner, M. (2002). Terminal differentiation of myelin-forming oligodendrocytes depends on the transcription factor Sox10. *Genes & development*, *16*(2), 165–170. https://doi.org/10.1101/gad.215802

Wegner M. (2008). A matter of identity: transcriptional control in oligodendrocytes. *Journal of molecular neuroscience: MN*, *35*(1), 3–12. https://doi.org/10.1007/s12031-007-9008-8

Wolf, N. I., Sistermans, E. A., Cundall, M., Hobson, G. M., Davis-Williams, A. P., Palmer, R., Stubbs, P., Davies, S., Endziniene, M., Wu, Y., Chong, W. K., Malcolm, S., Surtees, R., Garbern, J. Y., & Woodward, K. J. (2005). Three or more copies of the proteolipid protein gene PLP1 cause severe Pelizaeus-Merzbacher disease. *Brain: a journal of neurology*, *128*(Pt 4), 743–751. https://doi.org/10.1093/brain/awh409

Wei, Q., Miskimins, W. K., & Miskimins, R. (2004). Sox10 acts as a tissue-specific transcription factor enhancing activation of the myelin basic protein gene promoter by p27Kip1 and Sp1. *Journal of neuroscience research*, *78*(6), 796–802. https://doi.org/10.1002/jnr.20342

Xiao, S., Zhao, T., Wang, J., Wang, C., Du, J., Ying, L., Lin, J., Zhang, C., Hu, W., Wang, L., & Xu, K. (2019). Gelatin Methacrylate (GelMA)-Based Hydrogels for Cell Transplantation: an Effective Strategy for Tissue Engineering. *Stem cell reviews and reports*, *15*(5), 664–679. https://doi.org/10.1007/s12015-019-09893-4

Xie, S., Yang, J., Huang, S., Fan, Y., Xu, T., He, J., Guo, J., Ji, X., Wang, Z., Li, P., Chen, J., & Zhang, Y. (2022). Disrupted myelination network in the cingulate cortex of Parkinson's disease. *IET systems biology*, *16*(3-4), 98–119. https://doi.org/10.1049/syb2.12043

Yin, X., Crawford, T. O., Griffin, J. W., Tu, P.h, Lee, V. M., Li, C., Roder, J., & Trapp, B. D. (1998). Myelin-associated glycoprotein is a myelin signal that modulates the caliber of myelinated axons. *The Journal of neuroscience: the official journal of the Society for Neuroscience*, *18*(6), 1953–1962. https://doi.org/10.1523/JNEUROSCI.18-06-01953.1998

Yin, H., Zhu, M., Wang, Y., Luo, L., Ye, Q., & Lee, B. H. (2022). Physical properties and cellular responses of gelatin methacryloyl bulk hydrogels and highly ordered porous hydrogels. *Frontiers in Soft Matter*, *2*. https://doi.org/10.3389/frsfm.2022.1101680

Zalc, B., Goujet, D., & Colman, D. (2008). The origin of the myelination program in vertebrates. *Current biology: CB*, *18*(12), R511–R512. https://doi.org/10.1016/j.cub.2008.04.010

Zhang, J., Liu, X., Ma, K., Chen, M., Xu, H., Niu, X., Gu, H., Wang, R., Chen, X., & Sun, H. (2021). Collagen/heparin scaffold combined with vascular endothelial growth factor promotes the repair of neurological function in rats with traumatic brain injury. *Biomaterials Science*, *9*(3), 745–764. https://doi.org/10.1039/c9bm01446b

Zhang, H., Xu, J., & Saijilafu (2021). The effects of GelMA hydrogel on nerve repair and regeneration in mice with spinal cord injury. *Annals of translational medicine*, *9*(14), 1147. https://doi.org/10.21037/atm-21-2874

Zhang, S., Zhu, X., Gui, X., Croteau, C., Song, L., Xu, J., Wang, A., Bannerman, P., & Guo, F. (2018). Sox2 Is Essential for Oligodendroglial Proliferation and Differentiation during Postnatal Brain Myelination and CNS Remyelination. *The Journal of neuroscience: the official journal of the Society for Neuroscience*, *38*(7), 1802–1820. https://doi.org/10.1523/JNEUROSCI.1291-17.2018

Zhao, C., Ma, D., Zawadzka, M., Fancy, S. P., Elis-Williams, L., Bouvier, G., Stockley, J. H., de Castro, G. M., Wang, B., Jacobs, S., Casaccia, P., & Franklin, R. J. (2015). Sox2 Sustains Recruitment of Oligodendrocyte Progenitor Cells following CNS Demyelination and Primes Them for Differentiation during Remyelination. *The Journal of neuroscience : the official journal of the Society for Neuroscience*, *35*(33), 11482–11499. https://doi.org/10.1523/JNEUROSCI.3655-14.2015

Zhou, Q., & Anderson, D. J. (2002). The bHLH transcription factors OLIG2 and OLIG1 couple neuronal and glial subtype specification. *Cell*, *109*(1), 61–73. https://doi.org/10.1016/s0092-8674(02)00677-3

Zhou, Z., Ye, P., Li, X. H., Zhang, Y., Li, M., Chen, Q. Y., Lu, J. S., Xue, M., Li, Y., Liu, W., Lu, L., Shi, W., Xu, P. Y., & Zhuo, M. (2021). Synaptic potentiation of anterior cingulate cortex contributes to chronic pain of Parkinson's disease. *Molecular brain*, *14*(1), 161. https://doi.org/10.1186/s13041-021-00870-y

Zhu, X., Zuo, H., Maher, B. J., Serwanski, D. R., LoTurco, J. J., Lu, Q. R., & Nishiyama, A. (2012). Olig2-dependent developmental fate switch of NG2 cells. *Development (Cambridge, England)*, *139*(13), 2299–2307. https://doi.org/10.1242/dev.078873

Zimmermann, D. R., & Dours-Zimmermann, M. T. (2008). Extracellular matrix of the central nervous system: from neglect to challenge. *Histochemistry and cell biology*, *130*(4), 635–653. https://doi.org/10.1007/s00418-008-